Cell Reports

Resource

Population-based high-throughput toxicity screen of human iPSC-derived cardiomyocytes and neurons

Graphical abstract

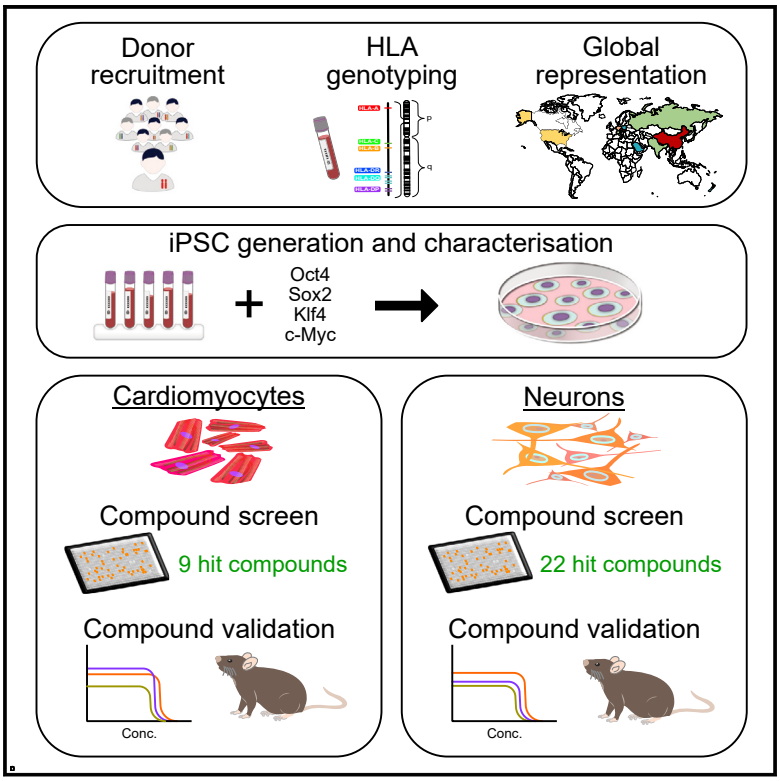

Highlights

- Development of a population-based iPSC cell bank
- Cell bank covers more than 477 million people worldwide based on HLA-A, HLA-B, and DRB1
- Population-based toxicity screen of iPSC-derived cardiomyocytes and neurons

Authors

Ching Ying Huang, Martin W. Nicholson, Jyun Yuan Wang, ..., Joseph C. Wu, Timothy J. Kamp, Patrick C.H. Hsieh

Correspondence

phsieh@ibms.sinica.edu.tw

In brief

Huang et al. use human leukocyte antigen as a genetic marker to identify representative donors that genetically represent the population of Taiwan. Their iPSCs are differentiated into cardiomyocytes and neurons to perform a population-based drug toxicity screen of compounds approved worldwide.

Huang et al., 2022, Cell Reports *39*, 110643
April 5, 2022 © 2022 The Author(s).
https://doi.org/10.1016/j.celrep.2022.110643

CellPress

Cell Reports

CellPress
OPEN ACCESS

Resource

Population-based high-throughput toxicity screen of human iPSC-derived cardiomyocytes and neurons

Ching Ying Huang,[1,9] Martin W. Nicholson,[1,9] Jyun Yuan Wang,[2] Chien Yu Ting,[1] Ming Heng Tsai,[1] Yu Che Cheng,[1] Chun Lin Liu,[1] Darien Z.H. Chan,[1] Yi Chan Lee,[1] Ching Chuan Hsu,[1] Yu Hung Hsu,[1] Chiou Fong Yang,[3] Cindy M.C. Chang,[4] Shu Chian Ruan,[1] Po Ju Lin,[1] Jen Hao Lin,[1] Li Lun Chen,[1] Marvin L. Hsieh,[1,4] Yuan Yuan Cheng,[1] Wan Tseng Hsu,[5] Yi Ling Lin,[1] Chien Hsiun Chen,[1] Yu Hsiang Hsu,[3] Ying Ta Wu,[2] Timothy A. Hacker,[4] Joseph C. Wu,[6] Timothy J. Kamp,[7] and Patrick C.H. Hsieh[1,7,8,10,*]

[1]Institute of Biomedical Sciences, Academia Sinica, Taipei 115, Taiwan
[2]Genomics Research Center, Academia Sinica, Taipei 115, Taiwan
[3]Institute of Applied Mechanics, National Taiwan University, Taipei 106, Taiwan
[4]Cardiovascular Physiology Core Facility, Department of Medicine, University of Wisconsin-Madison, Madison, WI 53705, USA
[5]School of Pharmacy, College of Medicine, National Taiwan University, Taipei 100, Taiwan
[6]Stanford Cardiovascular Institute, Stanford University School of Medicine, Stanford, CA 94305, USA
[7]Department of Medicine and Stem Cell and Regenerative Medicine Center, University of Wisconsin-Madison, Madison, WI 53705, USA
[8]Institute of Medical Genomics and Proteomics and Institute of Clinical Medicine, National Taiwan University, Taipei 106, Taiwan
[9]These authors contributed equally
[10]Lead contact
*Correspondence: phsieh@ibms.sinica.edu.tw
https://doi.org/10.1016/j.celrep.2022.110643

SUMMARY

In this study, we establish a population-based human induced pluripotent stem cell (hiPSC) drug screening platform for toxicity assessment. After recruiting 1,000 healthy donors and screening for high-frequency human leukocyte antigen (HLA) haplotypes, we identify 13 HLA-homozygous "super donors" to represent the population. These "super donors" are also expected to represent at least 477,611,135 of the global population. By differentiating these representative hiPSCs into cardiomyocytes and neurons we show their utility in a high-throughput toxicity screen. To validate hit compounds, we demonstrate dose-dependent toxicity of the hit compounds and assess functional modulation. We also show reproducible *in vivo* drug toxicity results using mouse models with select hit compounds. This study shows the feasibility of using a population-based hiPSC drug screening platform to assess cytotoxicity, which can be used as an innovative tool to study inter-population differences in drug toxicity and adverse drug reactions in drug discovery applications.

INTRODUCTION

Drug toxicity is a major cause of withdrawal of post-market drugs. Between 1953 and 2013, 462 medicinal products were withdrawn, with cardiotoxicity and neurotoxicity responsible for approximately 16% and 10%, respectively (Onakpoya et al., 2016; Siramshetty et al., 2016). The average research and development cost to bring a therapeutic agent to the market between 2009 and 2018 was estimated to be $1.3 billion. A major reason for such high costs is the high rate of failure during the development and clinical trial process. Only 25% of cardiovascular drugs and 15% of drugs for the central nervous system pass phase 1 clinical trials (Fogel, 2018; Wouters et al., 2020).

Population differences in adverse drug reactions and cytotoxicity have been reported extensively. In most cases, however, these are reported only after the drug has reached the market. For example, to reduce adverse drug reactions associated with warfarin, the dose for Asian individuals is lower than that for Caucasian individuals (Dang et al., 2005). A similar situation exists for other drugs, such as the β-blocker carvedilol and cardiovascular statin drugs (Liao, 2007; Tomlinson et al., 2018). Similarly, the anxiolytic drug diazepam is generally prescribed to Asian people at lower doses because of the differences in drug metabolism (Kim et al., 2004; Lin et al., 1988). Unfortunately, these adverse drug reactions are not detected during the drug development and clinical trial process because of a lack of population-specific models. Currently, the only population-based platforms available to test for such differences are *in silico* prediction models of drug toxicity (Jamei, 2016) and human lymphoblast cell lines. The human lymphoblast model is currently the only *in vitro* population-based drug screening model available (Abdo et al., 2015; Chiu et al., 2017).

Previously, most preclinical drug toxicity screening has relied heavily on immortalized cell lines and animal models. However, advances in cell technologies, such as human induced pluripotent stem cells (hiPSCs) (Matsa et al., 2014; Takahashi et al.,

This is an open access article under the CC BY-NC-ND license (http://creativecommons.org/licenses/by-nc-nd/4.0/).

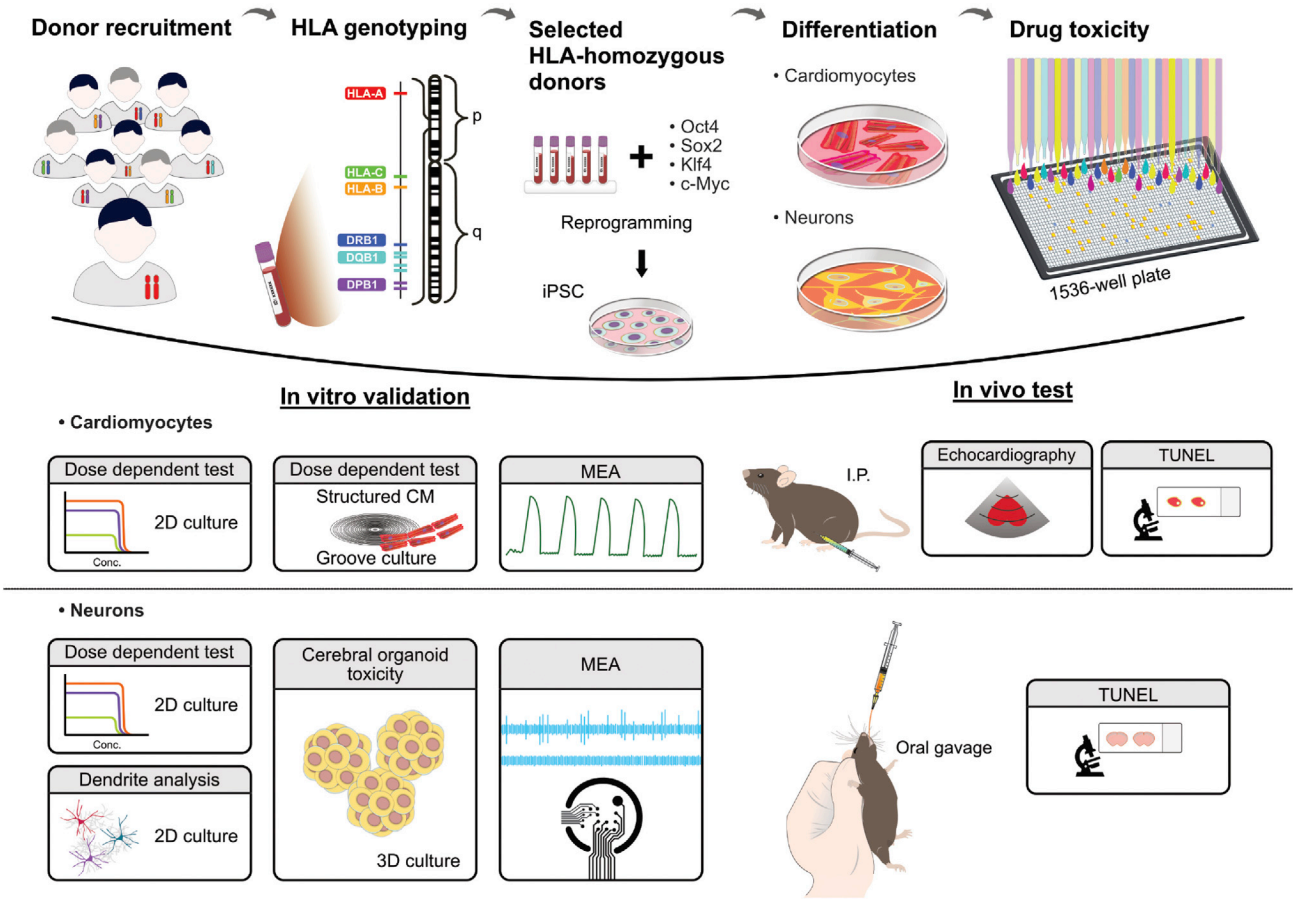

Figure 1. Schematic overview of the project

2007), allow more relevant platforms that more accurately model human physiology (Ronaldson-Bouchard and Vunjak-Novakovic, 2018; Sharma et al., 2020; Theodoris et al., 2021). It has been shown that hiPSC derivatives are an attractive model for cell toxicity assessment during drug development because of their biological relevance, specificity, and consistency (Burridge et al., 2016a; Doulatov et al., 2017; Sharma et al., 2017). hiPSC-derived cells retain the donor's genetic background and, thus, can mimic an individual's unique drug response; therefore, the US Food and Drug Administration (FDA) has encouraged use of hiPSCs as a human-relevant drug toxicity tool (Pang et al., 2019). hiPSCs are an unlimited source of human cells that can be differentiated into any cell type, such as cardiomyocytes, neurons, and hepatocytes, that can be used for high-throughput drug toxicity assessment and development (Ben-David et al., 2013; Coll et al., 2018; Tohyama et al., 2013; Vatine et al., 2019).

With limited population-based drug screening studies available, there is substantial interest in population-based hiPSC banks that can be employed in precision medicine, drug development, and drug screening studies (Sharma et al., 2017; Warren and Cowan, 2018). In this study, we generated a Chinese bank of human leukocyte antigen (HLA)-homozygous hiPSCs that represent ~16% of the population in Taiwan based on previously published HLA-A, HLA-B, and HLA-DRB1 haplotype frequency (Lai et al., 2010). This population-based cell bank was employed to perform a high-throughput cardio and neurotoxicity screen of clinically approved compounds to identify cardio- and neurotoxic compounds. The high cost of drug development combined with the high rate of drug withdrawal from the market indicates a need for a highly robust platform for drug screening that not only predicts drug toxicity in humans but can act as "phase 0" clinical trial during the drug development process.

RESULTS

Project workflow

Figure 1 summarizes the experimental design of our study. We aimed to establish a population-based drug toxicity screening platform. We recruited healthy donors and identified HLA-homozygous donors as population-representative donors. Peripheral blood mononuclear cells (PBMCs) from these representative donors were reprogrammed and differentiated into cardiomyocytes or neurons for further drug toxicity screening. Hit validation included *in vitro* assays such as dose-dependent assays and electrophysiological evaluation. We performed *in vivo* toxicity assessment using a terminal deoxynucleotidyl transferase dUTP-mediated nick-end labeling (TUNEL) assay to indicate cardiotoxicity and neurotoxicity.

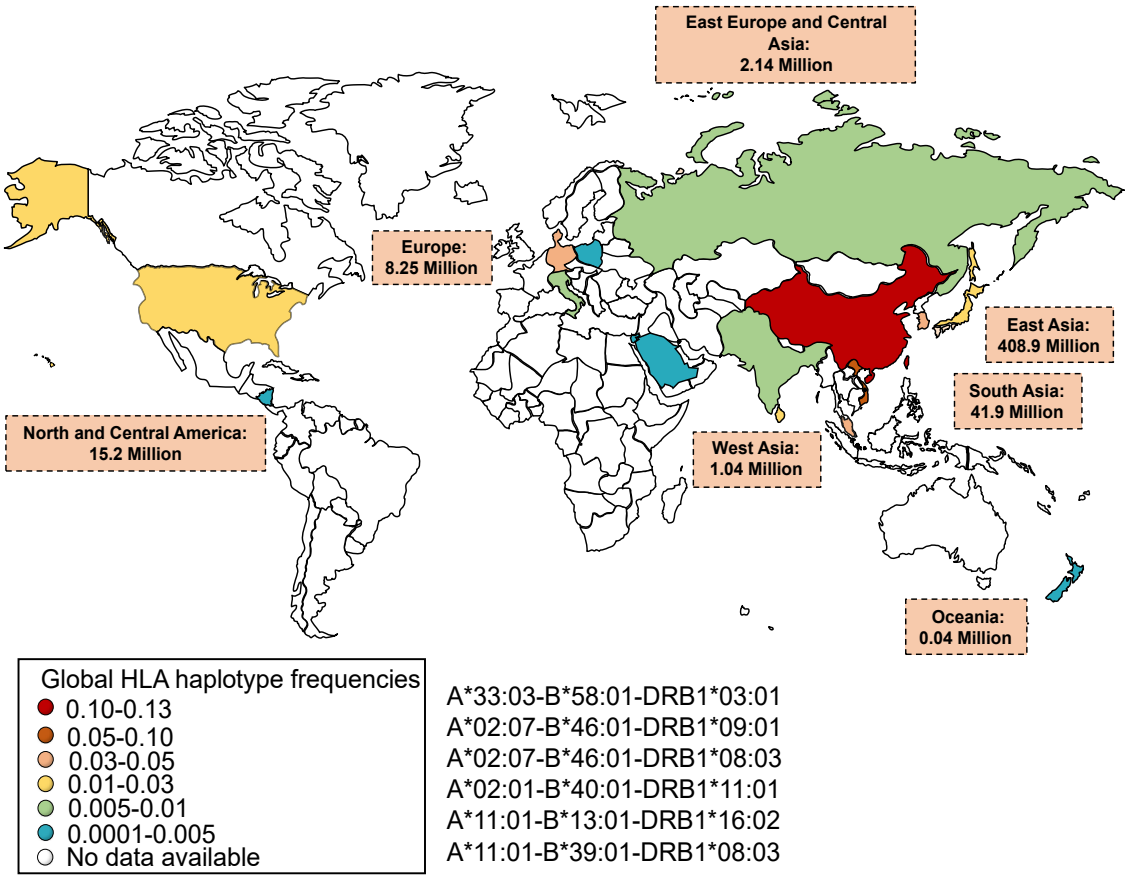

Figure 2. Map of worldwide coverage of representative HLA haplotype frequencies

Shown is a world map depicting the allele frequency of the 13 HLA-homozygous hiPSC lines globally with regional population coverage. The various colors indicate different ranges of haplotype frequencies, and the numbers in the boxes show the population coverage by continent.

Identification of HLA-homozygous donors from Taiwan

Previous reports have shown that differences in drug response exist between various populations because of genetic variation and that these differences can lead to adverse drug reactions to medical treatments (Dang et al., 2005; Kim et al., 2004). Using HLA as a population marker, we successfully identified 13 HLA-homozygous donors to represent the population. Overall, 6 donors were homozygous for 8 loci, 1 donor was homozygous for 7 loci, and 6 donors were homozygous for 6 loci. Details of the donor status are shown in Table S1. The donors' HLA haplotype frequency was ranked according to previously published HLA-A, HLA-B, and DRB1 haplotype frequencies in Taiwan (Table S2; Lai et al., 2010). These HLA-homozygous donor PBMCs were collected and reprogrammed into iPSCs for further study.

To understand the global HLA haplotype frequencies and population coverage of our representative HLA-homozygous hiPSCs, HLA-A, HLA-B, and DRB1 haplotype frequency data were obtained from the Allele Frequency Net Database (Gonzalez-Galarza et al., 2020). Figure 2 shows the global population coverage based on our HLA-homozygous hiPSC haplotypes. In total, our 13 representative HLA-homozygous hiPSC lines are able to cover 477,611,135 people of the 3,893,451,075 total population available from the Allele Frequency Net Database.

Generation and characterization of representative HLA-homozygous hiPSC lines

All representative donor PBMCs were reprogrammed by expression of Oct4, Sox2, Klf4, and c-Myc using the Sendai virus delivery method. All hiPSC lines were transgene free (Figure S1A) and represented a normal karyotype (Figure S1B). Immunofluorescence staining and confocal microscopy confirmed endogenous expression of various pluripotent markers, such as SSEA-4, TRA-1-60, OCT4, and SOX2 (Figure S1C). An *in vivo* teratoma formation assay revealed that all hiPSC lines formed teratomas and differentiated into ectoderm, mesoderm, and endoderm tissues (Figure S1D). We also used a short tandem repeat-based method to determine cell identity and performed PCR sequencing-based typing (SBT) to confirm that the HLA of the hiPSCs matched their original PBMCs (Table S1).

Validation of the population-based cardiotoxicity screening platform

To develop a 1,536-well plate-based cardiotoxic screening platform with population-representative hiPSC-derived cardiomyocytes (hiPSC-CMs), we differentiated all representative hiPSCs into CMs. The percentage of troponin-I-positive cells across each representative hiPSC-CM line (Figure S2B) averaged

95% ± 0.54% (Figure S2A). Prolonged culture of hiPSC-CMs has been shown to result in a more structurally mature phenotype. Analysis of α-actinin immunostaining of day 23 and day 47 hiPSC-CMs revealed a significantly longer sarcomere length in day 47 hiPSC-CMs than in day 23 hiPSC-CMs, indicating a more structurally mature phenotype (Figures S2C and S2D). We also tested the engraftment ability of iPSC-derived CMs into the mouse myocardium. We assessed whether these cells were able to survive *in vivo* while expressing the heart-specific marker α-actinin. A diagram of the cell engraftment assay is shown in Figure S2E. After engraftment for 3 weeks, an analysis revealed that all hiPSC-CM lines successfully engrafted into mouse hearts (Figure S2F). Engrafted cells were positive for human mitochondria, suggesting that all graft cells were human-derived cells (Figure S2G).

To investigate the effect of approved compounds on hiPSC-CM viability, a robust 1,536-well, high-content, high-throughput cardiotoxicity screening and hit validation was performed; an overview is shown in Figure 3A. All 13 representative HLA-homozygous hiPSC-CM lines were used for cardiotoxicity assessment. Three days after plating, 2,375 approved compounds were used to treat cells. Hit selection criteria were based on inducing more than 80% cardiotoxicity, after normalization with the vehicle group, in more than 3 hiPSC-CM cell lines. A representative image of a 1,536-well plate after treatment, staining, and imaging is shown in Figure 3A. In total, we identified 16 hit compounds (Table S3) as having cardiotoxic effects. Interestingly, in our screen, we identified a market-withdrawn drug, dithiazanine iodide, as cardiotoxic; it induced more than 80% cardiotoxicity in all representative lines.

Fifteen representative hit compounds (excluding dithiazanine iodide) were selected for further validation by assessing their dose-response toxicity effects. We observed a decrease in cell viability in 9 of the 15 compounds (pyrvinium, lapatinib, didrovaltrate, ethacridine lactate, valtrate, cetrorelix, idarubicin, doxorubicin, and daunorubicin) in all representative lines using a CellTiter-Glo assay (Figures 3B and S3). In total, we identified 5 previously known cardiotoxic drugs, including doxorubicin (Zhang et al., 2012), idarubicin (Anderlini et al., 1995), and lapatinib (Perez et al., 2008), and 4 previously undescribed cardiotoxic drugs. These drugs were then classified by their previous therapeutic use (Figure 3C; Table S4). We then used these validated compounds to assess the intra-donor variability using 2 cell lines and 3 clones from each line. We assessed the IC50 values for each clone and each drug and found no significant differences (Figures S3B and S3C). We confirmed these dose-dependent cytotoxic effects on structured hiPSC-CMs. Previous studies have shown that CMs cultured on a microgroove device can promote more maturely structured CMs (Huang et al., 2020; Lundy et al., 2013). A diagram of the 96-well microgroove plate is shown in Figure 3D. hiPSC-CMs cultured on the microgroove device showed a better alignment and elongation shape in the direction of the grooves compared with the no-groove group. When hiPSC-CMs were cultured on the no-groove surface, cells made contacts indiscriminately with neighboring cells. However, cells cultured on a grooved device had junctions that were less indiscriminately localized than those on a no-groove surface (Figure 3E). Similar to the monolayer culture, a clear dose-dependent decrease in viability was observed after compound treatment when cells were grown on a microgroove-structured plate (Figure 3F).

Electrophysiological effects of validated cardiotoxic compounds

From our validated compound list, we selected two drugs previously unidentified as cardiotoxic, valtrate and pyrvinium, to evaluate their effect on the function of hiPSC-CMs by investigating their electrophysiological effect on 3 cell lines using a multi-electrode array (MEA; Figure 4A). These 3 cell lines are representative of the population because they have the highest HLA haplotype frequency within the population. Valtrate treatment did not affect the field potential duration (FPD) and beat period; however, it induced a dose-dependent effect on the amplitude in 2 representative lines. In contrast, pyrvinium increased the FPD and beat period in all 3 representative lines in a dose-dependent manner. Pyrvinium decreased the amplitude in 2 representative hiPSC-CM lines. These data suggest that these drugs not only affect cell viability but also CM electrophysiology.

In vivo evaluation of validated cardiotoxic compounds

Next we assessed the *in vivo* toxicity of valtrate and pyrvinium. The experimental design of functional evaluation *in vivo* is shown in Figure 4C. The results showed that the end-systolic volume (ESV) and end-diastolic volume (EDV) decreased significantly after valtrate treatment, suggesting that valtrate induced myocardial strain after injection. However, pyrvinium treatment did not affect cardiac function (Figure 4D). In addition, a TUNEL assay was used to detect cell death *in vivo* after drug treatment. TUNEL-positive cells were detected in valtrate- and pyrvinium-treated mice. Fluorescein isothiocyanate (FITC)-labeled wheat germ agglutinin (WGA) was used to highlight cardiac myocyte borders; thus, only TUNEL-positive CMs were quantified. Figure 4E shows representative images; arrowheads indicate TUNEL-positive CMs. These data demonstrate that valtrate (4.7% ± 0.7%) and pyrvinium (7.2% ± 2.4%) treatment significantly induced CM cell death compared with the vehicle control (Figure 4F).

Generation and validation of the population-based high-throughput neurotoxicity screening platform

Because neurological complications are a leading cause of drug withdrawal from the market, we performed a population-based neurotoxicity screen using the same 13 HLA-homozygous hiPSC lines. The hiPSC lines were first differentiated into neuronal stem cells (hiPSC-NSCs). To assess their *in vivo* differentiation capability, the hiPSC-NSCs were engrafted into the subventricular zone of mice for 6 weeks (Figure S4A). Immunocytochemistry and confocal microscopy analysis revealed that all 13 hiPSC-NSC lines were positive for MAP2 (not expressed by hiPSC-NSCs) and human mitochondrion double-positive cells, showing their *in vivo* differentiation capability (Figures S4B and S4C). Concurrently, the hiPSC-NSCs were differentiated into neurons (hiPSC-NEURs) *in vitro*. The purity of the hiPSC-NEURs was confirmed by flow cytometry, shown as the percentage of MAP2- and NeuN-positive cells (Figure S4D). We found that the majority of the cells were glutamatergic, with a small

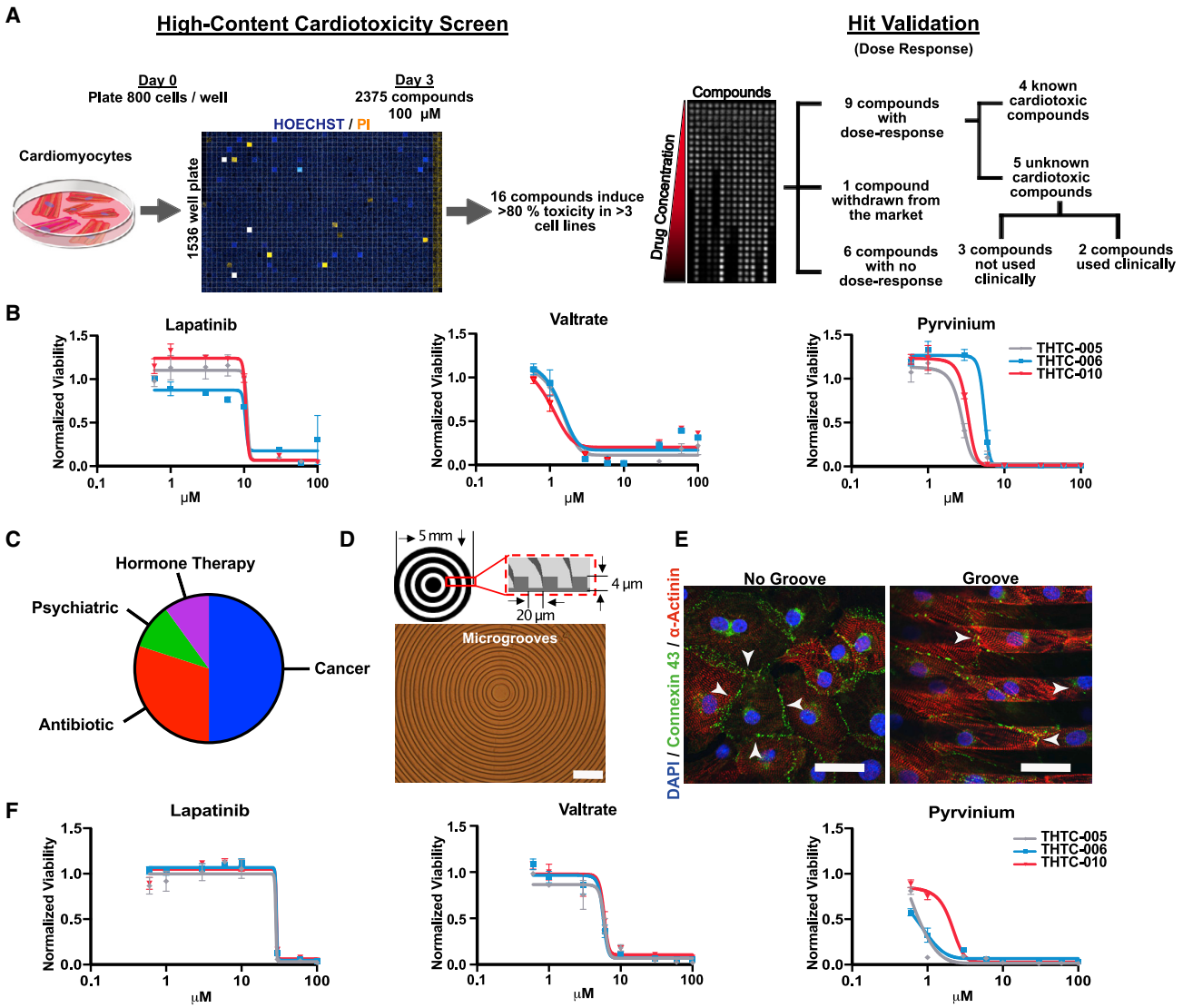

Figure 3. Identification and validation of cardiotoxic compounds from an approved drug library

(A) Experimental overview of high-throughput, high-content imaging and hit validation using hiPSC-CMs. Shown is high-content imaging of a 1,536-well plate after drug treatment and Hoechst 33342 (blue) and PI (orange) staining and the selection process of hit compounds.

(B) Comparative evaluation of cell viability by CellTiter-Glo assay of 3 representative HLA-homozygous cell lines after 24-h exposure for validation of hit compounds. Data represent triple repeats.

(C) Validated compounds characterized by their clinical indication.

(D) Diagram of the microgroove pattern on a 96-well plate. Scale bar, 40 µm.

(E) Immunocytochemistry analysis of CMs labeled with α-actinin (red), connexin 43 (green), and DAPI (blue) and plated on 96-well plate with and without grooves. Scale bars, 40 µm.

(F) Comparative evaluation of cell viability by CellTiter-Glo assay of cells plated onto a groove device for 3 representative cell lines treated for 24 h with pyrvinium, lapatinib, or didrovaltrate. Data represent triplet repeats. All data were obtained from studies performed in triplicate and represent mean ± SEM. See also Figures S2 and S3 and Tables S3 and S4.

population of GABAergic cells and no TH-positive (dopaminergic) cells in our cultures (Figure S4E). To assess the activity of the hiPSC-NEURs, live-cell calcium imaging revealed spontaneous calcium transients, indicating spontaneous neuronal activity in all 13 hiPSC-NEUR lines (Figure S4F). To better understand the maturity of the hiPSC-NEURs, we assessed the frequency and amplitude of spontaneous excitatory postsynaptic potentials, induced action potential frequency, and resting membrane potential using patch-clamp electrophysiology (Figure S4G).

After characterization of hiPSC-NEURs, we screened an FDA-approved compound library consisting of 2,080 compounds. From the primary screen, we selected 30 putative hits, derived from the top 1% toxic compounds found in at

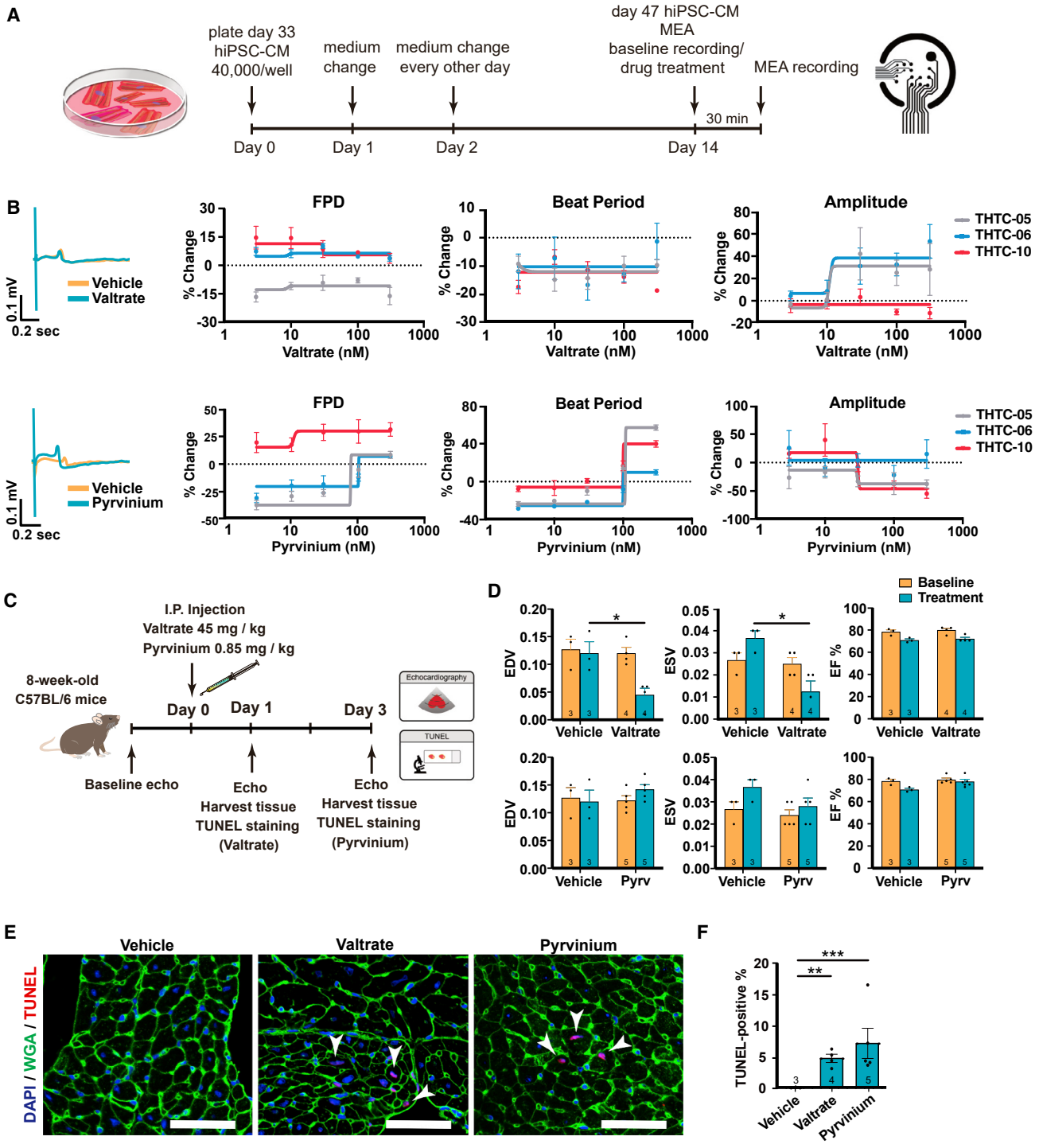

Figure 4. Functional evaluation of cardiotoxic compounds

(A) Timeline of MEA plating and drug treatment.

(B) MEA analysis of cardiotoxic compounds. FPD, field potential duration.

(C) Schematic of the *in vivo* cardiotoxicity analysis.

(D) Echocardiogram assessment. EDV, end-diastolic volume; ESV, end-systolic volume; EF, ejection fraction. Student's t test was used for statistical analysis. *$p < 0.05$.

(E) Fluorescence analysis of TUNEL staining of a mouse heart after drug treatment.

(F) Quantification of TUNEL-positive CMs after drug treatment. Statistical analysis was performed by ANOVA. Bars represent mean ± SEM. **$p < 0.01$, ***$p < 0.001$. Numbers within bars represent numbers of mice.

CellPress
OPEN ACCESS

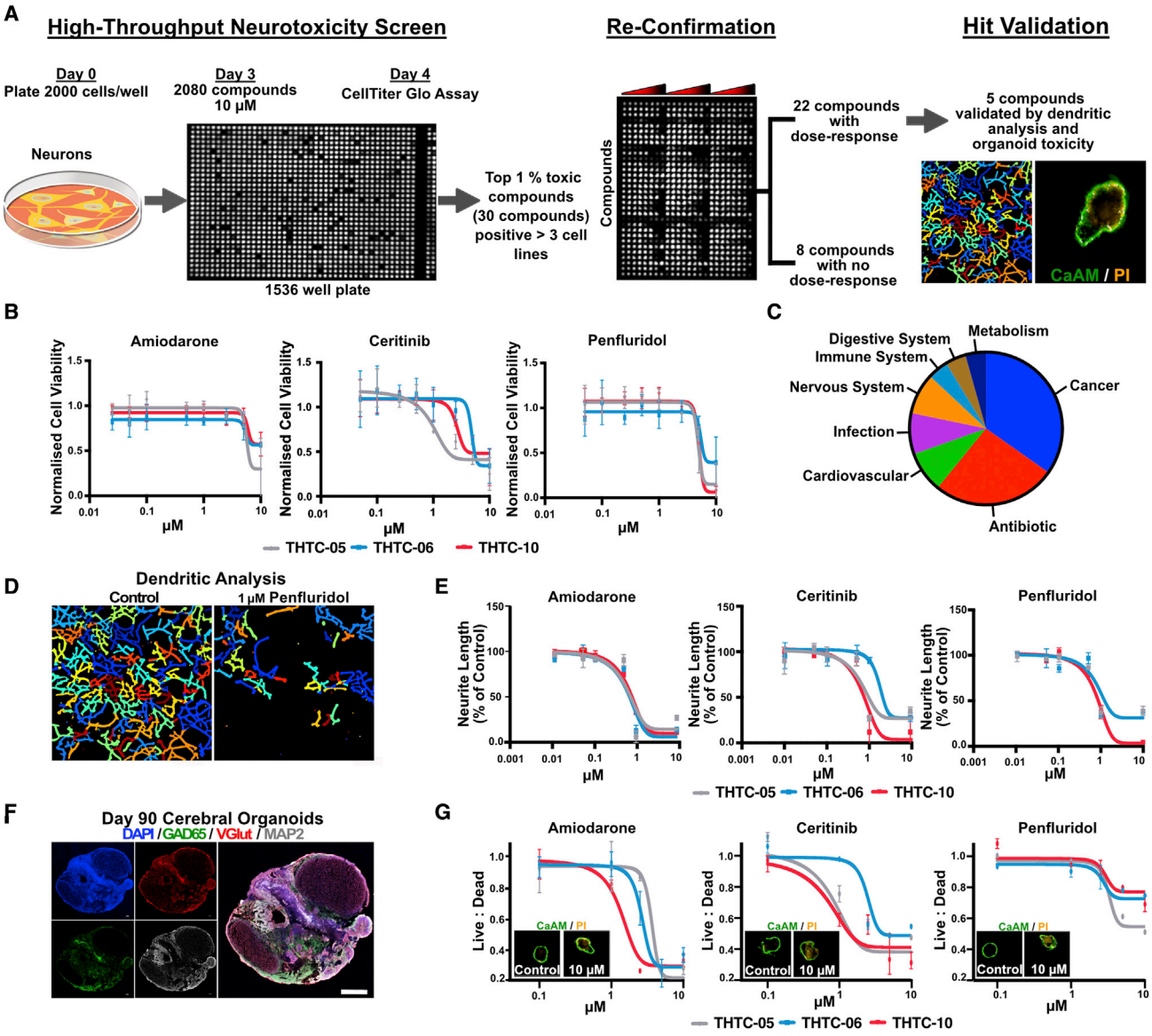

Figure 5. Identification and validation of neurotoxic compounds from an FDA-approved drug library

(A) Diagram of the experiment.

(B) Comparative evaluation of cell viability by CellTiter-Glo assay of 13 HLA-homozygous cell lines after 24-h exposure of hit compounds. Data represent assays conducted in triplicate.

(C) Reconfirmed compounds characterized by their clinical indication.

(D) Images of dendrite identification, using the CellProfiler plugin software, of control and treated neurons on a 96-well plate.

(E) Quantification of neurite length of the representative cell lines after 24-h drug treatment. Data were obtained from assays conducted in triplicate.

(F) Immunocytochemical labeling of GABAergic neurons (GAD65, green), glutamatergic neurons (VGLUT, red), mature neurons (MAP2, white) and DAPI (blue) in 90-day cerebral organoids. Scale bar, 0.5 mm.

(G) Quantification of calcein-AM:PI ratio in day 90 cerebral organoids after 24-h drug treatment. Inset: images generated from high-content analysis of organoids stained with the live cell stain calcein-AM (CaAM; green) and dead cell stain propidium iodide (PI; orange) of control and treated cerebral organoids. All data were obtained from assays conducted in triplicate and are represented as mean ± SEM.

See also Figures S4 and S5 and Tables S5 and S6.

least three cell lines (Table S5). The putative hits were reconfirmed by dose-response curves; of the 30 hit compounds, 22 compounds showed a dose-response toxicity relationship (Figures 5A, 5B, and S5A), 3 of which were known previously to be neurotoxic. To assess the intra-donor variability of these drugs, we tested 3 clones from 2 cell lines. The IC50 values were compared between clones for each drug. We found significant variability between IC50s in clones of THTC-05 treated

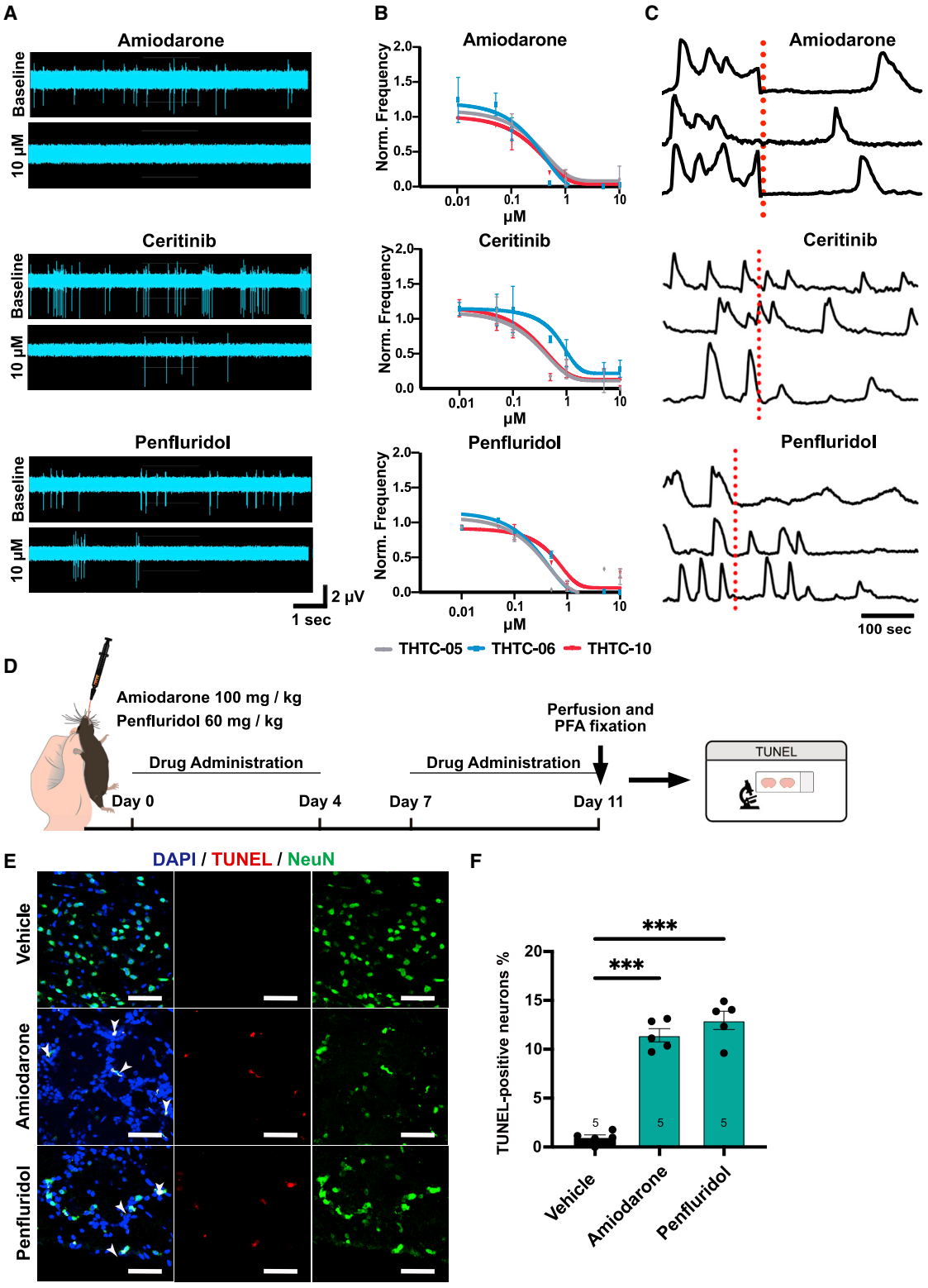

Figure 6. Validation of neurotoxic compounds

(A) Microelectrode array (MEA) traces of baseline recording (before drug treatment) and recordings after treatment for 30 min with 10 µM compound.

(B) Quantification of the frequency (hertz) of spontaneous action potentials using MEA after 30-min drug treatment in three cell lines.

(C) Examples of live-cell calcium imaging of day 80–90 cerebral organoids. The red line indicates addition of 10 µM drug.

(legend continued on next page)

with gramicidin and telotristat ethyl (Figure S5E). For all other drugs, we found no significant differences in IC50 values. We also assessed the effect of DMSO and found no significant differences in DMSO response (Figures S5B and S5C). The reconfirmed compounds were classified by their clinical indication, and the majority were anti-cancer drugs (Figure 5C; Table S6). Three compounds, amiodarone, ceritinib, and penfluridol, were selected for further validation based on their frequency of clinical use, potential application for repurposing, and previous evidence of crossing the blood-brain barrier (Petrelli et al., 2018; Riva et al., 1982; Tuan and Lee, 2019). Because dendritic complexity is a measure of cell health, we employed high-content imaging to validate these compounds by assessing the dendritic area after drug treatment. Employing the Cell Profiler plug-in (Carpenter et al., 2006), high-content images were generated for each condition, and dendrites were traced (Figures 5D and 5E). All compounds showed a dose-dependent loss of dendritic length and area in the 3 representative cell lines tested after drug treatment demonstrating the toxicity of these drugs (Figure 5E).

To further validate these drugs, we generated hiPSC-derived cerebral organoids. Because organoids have been shown to contain more mature neurons and to be structurally more complex, they better represent the *in vitro* characteristics of the brain compared with a traditional 2D culture (Jacob et al., 2020; Lancaster and Knoblich, 2014). Immunocytochemistry analysis showed that day 80–90 cerebral organoids were mainly positive for GABAergic and glutamatergic neurons (Figures 5F and S6). They contain GFAP- and SOX2-positive cells as well as a small population of TH-positive (dopaminergic) neurons (Figure S6). Therefore, day 80–90 cerebral organoids were employed to further validate hit compounds by dose-response analysis. After drug treatment, using live-dead stains (calcein-AM and propidium iodide [PI]; Figure 5G, inset), there was a dose-dependent decrease in the calcein-AM and PI ratio (Figure 5G), indicating loss of cell viability with increasing drug concentration.

Assessment of neuromodulation by hit compounds

Next, we monitored activity after amiodarone, ceritinib, and penfluridol treatments using MEA. Figure 6A shows representative traces of baseline and drug-treated field potential spikes. Quantification revealed that these compounds reduced the frequency of spontaneous neuronal activity (Figure 6B). These drugs were tested using live-cell calcium imaging of day 80–90 organoids. Similar to the MEA data from the 2D cultures, the hiPSC-derived cerebral organoids had a reduced frequency and amplitude of calcium peaks after 10 μM drug application (Figure 6C). These data show that amiodarone, ceritinib, and penfluridol reduce neuronal activity.

In vivo neurotoxicity

To confirm the *in vivo* toxicity of amiodarone and penfluridol, C57BL/6 mice were administered amiodarone (100 mg/kg/day) or penfluridol (60 mg/kg/day) by oral gavage for 11 days (Figure 6D). NeuN, used to identify neuronal nuclei, allowed identification of TUNEL-positive neurons, indicated by arrowheads in representative images (Figure 6E). Whole-brain sagittal sections were initially assessed, and quantification revealed a significant increase in TUNEL-positive neuronal nuclei after amiodarone (11% ± 0.7%) and penfluridol (13% ± 0.9%; Figure 6F) treatment compared with vehicle control. TUNEL-positive cells were mainly observed in the cortical region of the brain. These data demonstrate that amiodarone and penfluridol treatment induced neuron cell death *in vivo*.

Subpopulation differences in hit compound toxicity

We then assessed whether there were differences in subpopulations in response to the hit compounds. The IC50 values were calculated using GraphPad Prism. We found that idarubicin, doxorubicin, and daunorubicin showed cardiotoxic differences in subpopulations, mainly THTC-07. In doxorubicin-treated cells, we found that the average population of cells (all 13 lines) had a mean IC50 of 45 ± 4.4 μM, whereas THTC-07 had a significantly lower ($p < 0.01$) IC50 of 10 ± 0.5 μM (Figure 7A). Daunorubicin also showed population differences. Compared with the population average (30 ± 0.1 μM), THTC-07 had a significantly ($p < 0.001$) lower IC50 (5.9 ± 0.7 μM; Figure 7B). Another anthracycline-family drug, idarubicin, also showed population differences. The population average was 29 ± 0.2 μM. This was significantly higher ($p < 0.001$) than THTC-02 (10 ± 0.1 μM), THTC-06 (10.7 ± 0.2 μM), THTC-07 (10 ± 0.1 μM), THTC-09 (11 ± 0.1 μM), and THTC-12 (11 ± 0.2 μM; Figure 7C). Similarly, we found that the average IC50 of zinc pyrithione in neurons (5 ± 0.8 μM) was significantly ($p < 0.01$) higher compared with THTC-02 (0.5 ± 0.1 μM) and THTC-06 (0.3 ± 0.1 μM; Figure 7D).

DISCUSSION

In this study, we generated a population-based HLA-homozygous hiPSC bank by screening 1,000 healthy donors in Taiwan. To date, there has been no study that has established a population-representative drug screening model to assess cytotoxicity.

Population-based cytotoxicity screening model

It is well known that different populations respond differently to drugs. Population-representative drug screens rely heavily on commercially available cell lines for drug testing that does not accurately represent a population (Blinova et al., 2017; Kopljar et al., 2018). One study used 27 commercially available hiPSC-CMs as a population-based model to address inter-individual variability in cardiotoxicity (Grimm et al., 2018). They found that cell lines have variable responses to reference compounds after treatment. However, these cell lines were randomly selected without taking population-representative markers into account; therefore, 23 of these hiPSC-CMs were Caucasian, 4 of them

(D) Timeline of drug administration for *in vivo* toxicity study.
(E) Quantification of TUNEL staining in the mouse cortex after drug treatment. Scale bars, 50 μm.
(F) Quantification of TUNEL-positive neurons in the cortex from 5 animals for each condition. Statistical analysis was performed using one-way ANOVA (***$p < 0.001$). Data represent mean ± SEM.

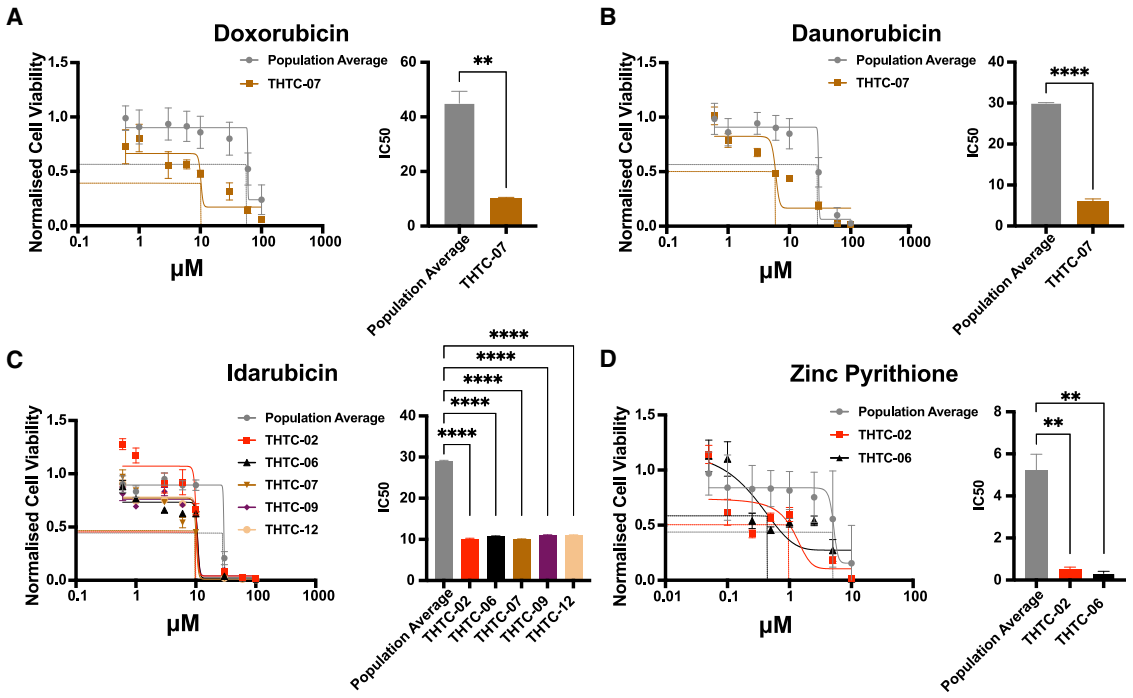

Figure 7. Sub-population differences in cardio and neurotoxicity

(A–C) Comparative evaluation of cardiotoxicity using a CellTiter-Glo assay of 13 HLA-homozygous cell lines after 24-h exposure of select hit compounds that show subpopulation differences in cardiotoxicity. Shown is the population average of all 13 lines and cell lines with significantly lower IC50 values of cardiotoxic compounds. Data represent assays conducted in triplicate.

(D) Neurotoxicity of zinc pyrithione in the average population (grey) and cell lines (red and black) has significantly lower IC50 values. Data represent assays conducted in triplicate. Bar graphs represent the mean ± SEM IC50 from the 13 cell lines. Statistical analysis was performed using unpaired t test (**$p < 0.01$, ****$p < 0.001$).

were African American, and Asian representation was completely absent.

Because Chinese people constitute the largest population in the world, we selected representative donors based on their HLA haplotype frequency within the population and established a population-based drug screening platform. It is well established that various populations exhibit different responses to warfarin; Chinese people in particular are known to be more sensitive to warfarin than Caucasians (Johnson, 2008; Lam and Cheung, 2012). Additionally, East Asians and Caucasians have different statin pharmacokinetics (Tomlinson et al., 2018). In our study, we found that different cell lines respond differently to the same drug; for example, didrovaltrate, idarubicin, and daunorubicin all displayed inter-individual differences in cardiotoxicity in their dose-response curves, whereas visomitin, ceritinib, and zinc pyrithione showed the greatest inter-individual differences in neurotoxicity. This may be explained by the intra-clone variability observed because there is an inherent variability between iPSC clones. Population-specific adverse drug reactions have been associated with the HLA complex. The HLA complex, which modulates the adaptive immune response, contains the most polymorphic genes in the human genome, and they are differentially expressed among populations. Evidence of this was reported in 2002, when HLA-B*57:01, most prevalent in Southeast Asian populations, was associated with abacavir sensitivity (Mallal et al., 2002). Additionally, allopurinol sensitivity resulting in Stevens-Johnson syndrome is strongly associated with HLA-B*58:01, which is found in 10%–15% of the Chinese population but only in 0.8% of the Caucasian population (Khanna et al., 2012; Lonjou et al., 2008). However, using this *in vitro* assay, we are unable to address HLA haplotype-specific toxicity directly. Apart from drug toxicity screening, this cell bank will have several important future implications for the use of hiPSCs in drug development and mechanistic studies.

We were unable to compare inter-population differences because of a lack of global effort to establish population-based hiPSC banks despite growing interest in population-based HLA-haplotype banking of hiPSCs (Nakajima et al., 2007; Taylor et al., 2012). There have been efforts by the Center for iPS Cell Research and Application in Japan, which has calculated that 5 HLA-homozygous hiPSC lines cover 32% of the population based on HLA-A, HLA-B, and HLA-DR (Umekage et al., 2019). This is possible because the Japanese population is relatively homogenous; however, Taiwan has a more diverse background. Based on previous HLA-B genotype results, our cell bank can cover ~51% of Taiwan's population, based solely on the HLA-B allele (Lai et al., 2010). Our results showed that these 13 representative hiPSC lines not only cover ~16% of Taiwan's population but can also cover over 477 million people in the world across various populations. It is important to note that these lines do not include the aboriginal peoples of Taiwan because they are a unique population that is genetically distinct

from the general population of Taiwan in terms of their HLA genotypes. Many other countries, such as the United States, also have a more genetically diverse population and, thus, may require more cell lines to represent their population. Clinical trials in iPSC-based cell therapy have seen promising results, starting in Japan (Mandai et al., 2017). Because HLA matching is important for organ transplantation and cell therapy to avoid rejection, having established cell banks with HLA-homozygous lines available would be an invaluable resource for clinicians and researchers. Although the iPSCs used in this study are not clinical-grade iPSCs, there is potential in reprogramming donor PBMCs into clinical-grade iPSCs for use in cell therapy and regenerative medicine.

Toxicity assessment and drug development

In this study, we successfully validated 9 approved compounds that induced cardiotoxicity and 22 compounds that induced neurotoxicity using this population-based toxicity screening platform. Although two different compound libraries were used, because availability, they both contained many of the same compounds. We have compared the compounds that induced cardiotoxicity and neurotoxicity and found that cardiotoxic compounds did not induce neurotoxicity and vice versa. Because we did not test other cell types, such as hepatocytes, we cannot comment on whether these compounds will induce toxicity in other cell types. Dithiazanine iodide induced cardiotoxicity in all of our representative hiPSC-CMs and, interestingly, was withdrawn from the market because of cardiovascular and metabolic reactions in 1964 (Qureshi et al., 2011). Several well-known anthracycline-induced cardiotoxic drugs were also identified in our study, such as daunorubicin, doxorubicin, and idarubicin (Anderlini et al., 1995; Burridge et al., 2016b; Lubieniecka et al., 2013; McGowan et al., 2017; Patnaik et al., 2011; Zhang et al., 2012). Previous studies have shown that iPSC-derived CMs can recapitulate doxorubicin-induced cardiotoxicity *in vitro* (Burridge et al., 2016b), and we identified subpopulations in our screen that were more sensitive (lower IC50) to these compounds. The THTC-07 line had greater sensitivity to all anthracycline drugs used in the study (doxorubicin, daunorubicin, and idarubicin). We also found that lapatinib induced cardiotoxicity, even though it showed low-level cardiotoxicity in clinical trials (Perez et al., 2008). This may indicate that inter-individual responses might be different in various populations. In addition to known cardiotoxic compounds, several unknown cardiotoxic compounds were identified, such as pyrvinium and didrovaltrate, found previously to block calcium currents in rabbit ventricular myocytes (Xie et al., 2012). Recently, studies have aimed to repurpose pyrvinium (an antihelmintic agent) as a cancer therapy drug because pyrvinium can interact with a complex of topoisomerase inhibitors and induce DNA damage (Chen et al., 2013). Although pyrvinium and valtrate induced cardiotoxicity *in vitro* and *in vivo*, there was little effect on heart function. Many of the TUNEL-positive cells were located close to the chamber of the heart, which may not immediately lead to impaired cardiac function; perhaps longer treatment regimens would result in more severe toxicity, leading to cardiac function impairment.

We were also able to identify previously known compounds with neurotoxic effects, such as zinc pyrithione, amiodarone, and moxidectin (Ménez et al., 2012; Nunes and Costa, 2019; Orr and Ahlskog, 2009). Although many drugs, in particular cancer drugs, have neurotoxic effects in peripheral nerves, we focused our study on toxicity of neurons found in the central nervous system, which usually manifests as cognitive impairment and seizures (Neurotoxicity of chemotherapy, 2007). Long-term use of amiodarone, a commonly prescribed anti-arrhythmic drug, has been shown to affect the central and peripheral nervous systems, including distal extremity weakness, loss of deep reflexes, and brain magnetic resonance imaging abnormalities (Van Herendael and Dorian, 2010). We observed a dose-dependent reduction in dendritic arborization after amiodarone treatment. Toxicity has been associated with axonal loss and demyelination; however, the mechanism of amiodarone-induced neurotoxicity is unknown (Galassi et al., 2014). Recently, penfluridol, an antipsychotic agent, has gained attention as a potential anti-cancer drug because it suppresses metastatic tumor growth (Ranjan and Srivastava, 2016). However, penfluridol crosses the blood-brain barrier (Ranjan et al., 2016), making it important to understand its potential neurological effects other than the associated antipsychotic effects. All drugs identified as toxic were classified by their clinical use. Demonstrating that anti-cancer drugs caused the most toxicity in hiPSC-CMs and hiPSC-NEURs shows the importance of developing more specific targeting methods for anti-cancer treatments. By employing single-cell genomics, we would be able to elucidate the target pathways involved in drug-induced toxicity, but this work focused on identifying toxic compounds. After toxicity evaluation, mechanistic studies could be undertaken to determine the specific pathways involved.

Traditional cell culture assays rely on 2D culturing systems, which provide valuable information; however, advancing culture techniques will allow more complex 3D cultures to be employed in high-throughput screens. More complicated cultures, such as organoids, microfluidics, and micro-patterned devices, are highly amenable to high-throughput screening; however, current methods require technical effort and important manipulations that have hindered progress. We found, in our assays, that the organoid cultures produced a result similar to 2D cultures with regard to toxicity, but they may provide more valuable information on how different compounds may alter neuronal pathways or networks resulting in, for example, excitotoxicity or development. Use of the microgroove device and organoids provides a more physiological relevant state of hiPSC-derived cells. This generates a more mature, *in-vivo*-like phenotype facilitating further drug toxicity tests or mechanistic studies. We also present an effective method for detecting toxicity in organoid cultures; however, culturing technology has not yet reached the high-throughput capacity of organoids and may only be employed for validation purposes.

CONCLUSION

With ever-evolving culture technologies, population-based hiPSC banks will allow advances in precision medicine. One of the barriers during drug development is the variation between current models used for testing; however, the risk of population-specific toxicities remains unknown. When population

hiPSC banks are developed, this platform can be used to investigate inter-population differences. This platform can also be used to screen for hepatotoxicity (Cayo et al., 2017). Between 1997 and 2016, 8 drugs were withdrawn from the market because of hepatotoxicity (Babai et al., 2018). The Comprehensive In Vitro Proarrhythmia Assay (CiPA) initiative has resulted in large-scale efforts by academia, industry, and regulatory bodies to advocate for use of hiPSC-CMs to predict the translational potential of drug-induced cardiac toxicity/arrhythmia. Unfortunately, such initiatives have yet to be implemented for hiPSC-NEURs. Our cell bank allows development of such guidelines not only for neurons but also hepatocytes. Finally, development of population-based hiPSC banks provides researchers and clinicians opportunities to avoid potential toxicity not detected by the current drug development pipeline.

Limitations of the study

This study demonstrates use of a population of hiPSCs defined by HLA; however, to determine population differences in drug responses or toxicity, other countries would be required to develop their own cohorts of HLA-defined hiPSCs. The linkage disequilibrium with the HLA haplotypes could include a variety of genes/loci, which may be a factor when investigating HLA-associated adverse reactions such as TNF (Sanchez-Mazas et al., 2000). It is important to note that HLA-associated adverse reactions generally rely on activation of the immune system; therefore, this *in vitro* assay would unlikely be able to detect HLA-specific toxicity. Collaborative efforts can then be undertaken to investigate population differences in drug toxicity. Because of the limitations connected to biosafety level 3, it will be important to test the toxicity of hiPSC-CMs after viral infection. Drugs that did not show toxicity in healthy hiPSC-CMs may display higher drug sensitivity in virus-infected cells. Although we identified previously known cardio- and neurotoxic compounds in the screen, the compound library database does not provide information on toxicity of the drugs contained in it; therefore, we are unable to validate whether the screening method identified all known cardio- and neurotoxic compounds.

STAR★METHODS

Detailed methods are provided in the online version of this paper and include the following:

- KEY RESOURCES TABLE
- RESOURCE AVAILABILITY
  - Lead contact
  - Materials availability
  - Data and code availability
- EXPERIMENTAL MODEL AND SUBJECT DETAILS
  - Human donors
  - Mice
- METHOD DETAILS
  - Donor recruitment
  - HLA typing
  - Global HLA haplotype frequencies and population coverage
  - Detection of sendai virus expression
  - Immunocytochemistry
  - Teratoma formation assay
  - Karyotyping analysis
  - Compound collections
  - Human iPSC generation
  - Cardiac differentiation
  - Cell culture and compound treatment for cardiotoxicity screening
  - Fabrication of a multi-well plate with embedded microgrooves
  - HiPSC-CM engraftment
  - Micro electro array
  - *In vivo* cardiotoxicity assay
  - Neuronal differentiation
  - Cerebral organoid generation
  - Cell culture and compound treatment for neurotoxicity screening
  - Dendrite analysis for neurotoxicity screening
  - *In vivo* neurotoxicity assay
  - *In vivo* neuronal differentiation
  - Electrophysiology
  - Live-cell calcium imaging
  - Statistical analysis

SUPPLEMENTAL INFORMATION

Supplemental information can be found online at https://doi.org/10.1016/j.celrep.2022.110643.

ACKNOWLEDGMENTS

We thank the Taiwan Human Disease iPSC Service Consortium for iPSC generation, the Translational Resource Center for Genomic Medicine (TRC) for donor recruitment, and the National Center for Genome Medicine for technical support. We thank Huei-Fang Wu in the Neuroscience Core Facility (supported by grant AS-CFII-110-101), Neuroscience Program of Academia Sinica, Academia Sinica for electrophysiology experiments. This study is supported by the Ministry of Science and Technology, Taiwan (109-2321-B-001-012, 109-2327-B-001-001, 109-2740-B-001-002, and MOST 110-2740-B-001-003), the National Health Research Institutes (EX109-10907SI), the Academia Sinica Healthy Longevity Grand Challenge (AS-HLGC-109-05), and the Translational Medical Research Program (AS-KPQ-110-BioMed).

AUTHOR CONTRIBUTIONS

P.C.H.H. conceived and supervised the project. C.Y.H. managed the study, performed HLA genotyping, analyzed genotyping data, and interpreted the results in consultation with C.H.C. C.Y.H. and M.W.N. designed experiments and contributed to data analysis and manuscript preparation. C.Y.H., Y.C.C., C.Y.T., Yu Hung Hsu, and C.L.L. recruited donors and generated iPSCs. C.Y.H., C.Y.T., M.H.T., J.H.L., M.L.H., and S.C.R. characterized iPSCs. C.Y.H., M.H.T., Y.C.C., C.Y.T., D.Z.H.C., and C.L.L. produced iPSC-derived CMs and banked iPSCs. C.Y.T. and M.W.N. produced and characterized iPSC-derived neurons. L.L.C. prepared the schematic illustrations. P.J.L. performed echography, and Y.Y.C. contributed to the *in vivo* toxicity assays. J.Y.W. and Y.T.W. contributed to high-throughput screening. W.T.H. contributed to hit classification and validation. C.F.Y. and Yu Hsiang Hsu designed the microgroove plate. C.M.C.C., T.A.H., J.C.W., and T.J.K. contributed to the concept and design of the study. All authors discussed the results, commented on the manuscript, and read and approved the final manuscript.

DECLARATION OF INTERESTS

The authors declare no competing interests.

Received: July 6, 2021
Revised: January 13, 2022
Accepted: March 16, 2022
Published: April 5, 2022

REFERENCES

Abdo, N., Xia, M., Brown, C.C., Kosyk, O., Huang, R., Sakamuru, S., Zhou, Y.-H., Jack, J.R., Gallins, P., Xia, K., et al. (2015). Population-based in vitro hazard and concentration-response assessment of chemicals: the 1000 genomes high-throughput screening study. Environ. Health Perspect. *123*, 458–466. https://doi.org/10.1289/ehp.1408775.

Anderlini, P., Benjamin, R.S., Wong, F.C., Kantarjian, H.M., Andreeff, M., Kornblau, S.M., O'Brien, S., Mackay, B., Ewer, M.S., Pierce, S.A., et al. (1995). Idarubicin cardiotoxicity: a retrospective study in acute myeloid leukemia and myelodysplasia. J. Clin. Oncol. *13*, 2827–2834. https://doi.org/10.1200/jco.1995.13.11.2827.

Babai, S., Auclert, L., and Le-Louet, H. (2018). Safety data and withdrawal of hepatotoxic drugs. Therapie *9*, eaah5645. https://doi.org/10.1016/j.therap.2018.02.004.

Ben-David, U., Gan, Q.F., Golan-Lev, T., Arora, P., Yanuka, O., Oren, Y.S., Leikin-Frenkel, A., Graf, M., Garippa, R., Boehringer, M., et al. (2013). Selective elimination of human pluripotent stem cells by an oleate synthesis inhibitor discovered in a high-throughput screen. Cell Stem Cell *12*, 167–179. https://doi.org/10.1016/j.stem.2012.11.015.

Blinova, K., Stohlman, J., Vicente, J., Chan, D., Johannesen, L., Hortigon-Vinagre, M.P., Zamora, V., Smith, G., Crumb, W.J., Pang, L., et al. (2017). Comprehensive translational assessment of human-induced pluripotent stem cell derived cardiomyocytes for evaluating drug-induced arrhythmias. Toxicol. Sci. *155*, 234–247. https://doi.org/10.1093/toxsci/kfw200.

Braun, R., Dittmar, W., Hubner, G.E., and Maurer, H.R. (1984). Influence of valtrate/isovaltrate on the hematopoiesis and metabolic liver activity in mice in vivo. Planta Med. *50*, 1–4. https://doi.org/10.1055/s-2007-969603.

Burridge, P.W., Diecke, S., Matsa, E., Sharma, A., Wu, H., and Wu, J.C. (2016a). Modeling cardiovascular diseases with patient-specific human pluripotent stem cell-derived cardiomyocytes. Methods Mol. Biol. *1353*, 119–130. https://doi.org/10.1007/7651_2015_196.

Burridge, P.W., Li, Y.F., Matsa, E., Wu, H., Ong, S.G., Sharma, A., Holmstrom, A., Chang, A.C., Coronado, M.J., Ebert, A.D., et al. (2016b). Human induced pluripotent stem cell-derived cardiomyocytes recapitulate the predilection of breast cancer patients to doxorubicin-induced cardiotoxicity. Nat. Med. *22*, 547–556. https://doi.org/10.1038/nm.4087.

Carpenter, A.E., Jones, T.R., Lamprecht, M.R., Clarke, C., Kang, I.H., Friman, O., Guertin, D.A., Chang, J.H., Lindquist, R.A., Moffat, J., et al. (2006). CellProfiler: image analysis software for identifying and quantifying cell phenotypes. Genome Biol. *7*, R100. https://doi.org/10.1186/gb-2006-7-10-r100.

Cayo, M.A., Mallanna, S.K., Di Furio, F., Jing, R., Tolliver, L.B., Bures, M., Urick, A., Noto, F.K., Pashos, E.E., Greseth, M.D., et al. (2017). A drug screen using human iPSC-derived hepatocyte-like cells reveals cardiac glycosides as a potential treatment for hypercholesterolemia. Cell Stem Cell *20*, 478–489.e475. https://doi.org/10.1016/j.stem.2017.01.011.

Chen, J., Kang, D., Xu, J., Lake, M., Hogan, J.O., Sun, C., Walter, K., Yao, B., and Kim, D. (2013). Species differences and molecular determinant of TRPA1 cold sensitivity. Nat. Commun. *4*, 2501. https://doi.org/10.1038/ncomms3501.

Chiu, W.A., Wright, F.A., and Rusyn, I. (2017). A tiered, Bayesian approach to estimating of population variability for regulatory decision-making. Altex *34*, 377–388. https://doi.org/10.14573/altex.1608251.

Coll, M., Perea, L., Boon, R., Leite, S.B., Vallverdu, J., Mannaerts, I., Smout, A., El Taghdouini, A., Blaya, D., Rodrigo-Torres, D., et al. (2018). Generation of hepatic stellate cells from human pluripotent stem cells enables in vitro modeling of liver fibrosis. Cell Stem Cell *23*, 101–113.e7. https://doi.org/10.1016/j.stem.2018.05.027.

Dang, M.-T.N., Hambleton, J., and Kayser, S.R. (2005). The influence of ethnicity on warfarin dosage requirement. Ann. Pharmacother. *39*, 1008–1012. https://doi.org/10.1345/aph.1E566.

Doulatov, S., Vo, L.T., Macari, E.R., Wahlster, L., Kinney, M.A., Taylor, A.M., Barragan, J., Gupta, M., McGrath, K., Lee, H.Y., et al. (2017). Drug discovery for Diamond-Blackfan anemia using reprogrammed hematopoietic progenitors. Sci. Transl Med. *9*, eaah5645. https://doi.org/10.1126/scitranslmed.aah5645.

Fogel, D.B. (2018). Factors associated with clinical trials that fail and opportunities for improving the likelihood of success: a review. Contemp. Clin. Trials Commun. *11*, 156–164. https://doi.org/10.1016/j.conctc.2018.08.001.

Galassi, G., Georgoulopoulou, E., and Ariatti, A. (2014). Amiodarone neurotoxicity: the other side of the medal. Cent. Eur. J. Med. *9*, 437–442. https://doi.org/10.2478/s11536-013-0306-y.

Gonzalez-Galarza, F.F., McCabe, A., Santos, E., Jones, J., Takeshita, L., Ortega-Rivera, N.D., Cid-Pavon, G.M.D., Ramsbottom, K., Ghattaoraya, G., Alfirevic, A., et al. (2020). Allele frequency net database (AFND) 2020 update: gold-standard data classification, open access genotype data and new query tools. Nucleic Acids Res. *48*, D783–D788. https://doi.org/10.1093/nar/gkz1029.

Grimm, F.A., Blanchette, A., House, J.S., Ferguson, K., Hsieh, N.H., Dalaijamts, C., Wright, A.A., Anson, B., Wright, F.A., Chiu, W.A., and Rusyn, I. (2018). A human population-based organotypic in vitro model for cardiotoxicity screening. ALTEX *35*, 441–452. https://doi.org/10.14573/altex.1805301.

Huang, C.Y., Li, L.H., Hsu, W.T., Cheng, Y.C., Nicholson, M.W., Liu, C.L., Ting, C.Y., Ko, H.W., Syu, S.H., Wen, C.H., et al. (2020). Copy number variant hotspots in Han Taiwanese population induced pluripotent stem cell lines - lessons from establishing the Taiwan human disease iPSC Consortium Bank. J. Biomed. Sci. *27*, 92. https://doi.org/10.1186/s12929-020-00682-7.

Huang, R., Zhu, H., Shinn, P., Ngan, D., Ye, L., Thakur, A., Grewal, G., Zhao, T., Southall, N., Hall, M.D., et al. (2019). The NCATS pharmaceutical collection: a 10-year update. Drug Discov. Today *24*, 2341–2349. https://doi.org/10.1016/j.drudis.2019.09.019.

Jacob, F., Pather, S.R., Huang, W.K., Zhang, F., Wong, S.Z.H., Zhou, H., Cubitt, B., Fan, W., Chen, C.Z., Xu, M., et al. (2020). Human pluripotent stem cell-derived neural cells and brain organoids reveal SARS-CoV-2 neurotropism predominates in choroid plexus epithelium. Cell Stem Cell *27*, 937–950.e939. https://doi.org/10.1016/j.stem.2020.09.016.

Jamei, M. (2016). Recent advances in development and application of physiologically-based pharmacokinetic (PBPK) models: a transition from academic curiosity to regulatory acceptance. Curr. Pharmacol. Rep. *2*, 161–169. https://doi.org/10.1007/s40495-016-0059-9.

Johnson, J.A. (2008). Ethnic differences in cardiovascular drug response: potential contribution of pharmacogenetics. Circulation *118*, 1383–1393. https://doi.org/10.1161/circulationaha.107.704023.

Khanna, D., Khanna, P.P., Fitzgerald, J.D., Singh, M.K., Bae, S., Neogi, T., Pillinger, M.H., Merill, J., Lee, S., Prakash, S., et al. (2012). 2012 American College of Rheumatology guidelines for management of gout. Part 2: therapy and antiinflammatory prophylaxis of acute gouty arthritis. Arthritis Care Res. (Hoboken) *64*, 1447–1461. https://doi.org/10.1002/acr.21773.

Kim, K., Johnson, J.A., and Derendorf, H. (2004). Differences in drug pharmacokinetics between East Asians and Caucasians and the role of genetic polymorphisms. J. Clin. Pharmacol. *44*, 1083–1105. https://doi.org/10.1177/0091270004268128.

Kopljar, I., Lu, H.R., Van Ammel, K., Otava, M., Tekle, F., Teisman, A., and Gallacher, D.J. (2018). Development of a human iPSC cardiomyocyte-based scoring system for cardiac hazard identification in early drug safety de-risking. Stem Cell Rep. *11*, 1365–1377. https://doi.org/10.1016/j.stemcr.2018.11.007.

Lai, M.J., Wen, S.H., Lin, Y.H., Shyr, M.H., Lin, P.Y., and Yang, K.L. (2010). Distributions of human leukocyte antigen-A, -B, and -DRB1 alleles and

haplotypes based on 46,915 Taiwanese donors. Hum. Immunol. *71*, 777–782. https://doi.org/10.1016/j.humimm.2010.05.013.

Lam, M.P., and Cheung, B.M. (2012). The pharmacogenetics of the response to warfarin in Chinese. Br. J. Clin. Pharmacol. *73*, 340–347. https://doi.org/10.1111/j.1365-2125.2011.04097.x.

Lancaster, M.A., and Knoblich, J.A. (2014). Generation of cerebral organoids from human pluripotent stem cells. Nat. Protoc. *9*, 2329–2340. https://doi.org/10.1038/nprot.2014.158.

Le Bouter, S., El Harchi, A., Marionneau, C., Bellocq, C., Chambellan, A., van Veen, T., Boixel, C., Gavillet, B., Abriel, H., Le Quang, K., et al. (2004). Long-term amiodarone administration remodels expression of ion channel transcripts in the mouse heart. Circulation *110*, 3028–3035. https://doi.org/10.1161/01.CIR.0000147187.78162.

Liao, J.K. (2007). Safety and efficacy of statins in Asians. Am. J. Cardiol. *99*, 410–414. https://doi.org/10.1016/j.amjcard.2006.08.051.

Lin, K.M., Lau, J.K., Smith, R., Phillips, P., Antal, E., and Poland, R.E. (1988). Comparison of alprazolam plasma levels in normal Asian and Caucasian male volunteers. Psychopharmacology (Berl) *96*, 365–369. https://doi.org/10.1007/BF00216063.

Liu, Y., She, P., Xu, L., Chen, L., Li, Y., Liu, S., Li, Z., Hussain, Z., and Wu, Y. (2021). Antimicrobial, antibiofilm, and anti-persister activities of penfluridol against Staphylococcus aureus. Front Microbiol. *12*, 727692. https://doi.org/10.3389/fmicb.2021.727692.

Lonjou, C., Borot, N., Sekula, P., Ledger, N., Thomas, L., Halevy, S., Naldi, L., Bouwes-Bavinck, J.N., Sidoroff, A., de Toma, C., et al. (2008). A European study of HLA-B in Stevens-Johnson syndrome and toxic epidermal necrolysis related to five high-risk drugs. Pharmacogenet Genomics *18*, 99–107. https://doi.org/10.1097/FPC.0b013e3282f3ef9c.

Lubieniecka, J.M., Graham, J., Heffner, D., Mottus, R., Reid, R., Hogge, D., Grigliatti, T.A., and Riggs, W.K. (2013). A discovery study of daunorubicin induced cardiotoxicity in a sample of acute myeloid leukemia patients prioritizes P450 oxidoreductase polymorphisms as a potential risk factor. Front Genet. *4*, 231. https://doi.org/10.3389/fgene.2013.00231.

Lundy, S.D., Zhu, W.Z., Regnier, M., and Laflamme, M.A. (2013). Structural and functional maturation of cardiomyocytes derived from human pluripotent stem cells. Stem Cells Dev *22*, 1991–2002. https://doi.org/10.1089/scd.2012.0490.

Mallal, S., Nolan, D., Witt, C., Masel, G., Martin, A.M., Moore, C., Sayer, D., Castley, A., Mamotte, C., Maxwell, D., et al. (2002). Association between presence of HLA-B*5701, HLA-DR7, and HLA-DQ3 and hypersensitivity to HIV-1 reverse-transcriptase inhibitor abacavir. Lancet *359*, 727–732. https://doi.org/10.1016/s0140-6736(02)07873-x.

Mandai, M., Kurimoto, Y., and Takahashi, M. (2017). Autologous induced stem-cell-derived retinal cells for macular degeneration. N. Engl. J. Med. *377*, 792–793. https://doi.org/10.1056/NEJMc1706274.

Matsa, E., Burridge, P.W., and Wu, J.C. (2014). Human stem cells for modeling heart disease and for drug discovery. Sci. Transl Med. *6*, 239ps236. https://doi.org/10.1126/scitranslmed.3008921.

McGowan, J.V., Chung, R., Maulik, A., Piotrowska, I., Walker, J.M., and Yellon, D.M. (2017). Anthracycline chemotherapy and cardiotoxicity. Cardiovasc. Drugs Ther. *31*, 63–75. https://doi.org/10.1007/s10557-016-6711-0.

Ménez, C., Sutra, J.F., Prichard, R., and Lespine, A. (2012). Relative neurotoxicity of ivermectin and moxidectin in Mdr1ab (-/-) mice and effects on mammalian GABA(A) channel activity. Plos Negl. Trop. Dis. *6*, e1883. https://doi.org/10.1371/journal.pntd.0001883.

Momtazi-Borojeni, A.A., Abdollahi, E., Ghasemi, F., Caraglia, M., and Sahebkar, A. (2018). The novel role of pyrvinium in cancer therapy. J. Cell Physiol *233*, 2871–2881. https://doi.org/10.1002/jcp.26006.

Nakajima, F., Tokunaga, K., and Nakatsuji, N. (2007). Human leukocyte antigen matching estimations in a hypothetical bank of human embryonic stem cell lines in the Japanese population for use in cell transplantation therapy. Stem Cells *25*, 983–985. https://doi.org/10.1634/stemcells.2006-0566.

(2007). Neurotoxicity of chemotherapy. Nat. Clin. Pract. Neurol. *3*, 125. https://doi.org/10.1038/ncpneuro0418.

Nunes, B., and Costa, M. (2019). Study of the effects of zinc pyrithione in biochemical parameters of the Polychaeta Hediste diversicolor: evidences of neurotoxicity at ecologically relevant concentrations. Environ. Sci. Pollut. Res. Int. *26*, 13551–13559. https://doi.org/10.1007/s11356-019-04810-1.

Onakpoya, I.J., Heneghan, C.J., and Aronson, J.K. (2016). Post-marketing withdrawal of 462 medicinal products because of adverse drug reactions: a systematic review of the world literature. BMC Med. *14*, 10. https://doi.org/10.1186/s12916-016-0553-2.

Orr, C.F., and Ahlskog, J.E. (2009). Frequency, characteristics, and risk factors for amiodarone neurotoxicity. Arch. Neurol. *66*, 865–869. https://doi.org/10.1001/archneurol.2009.96.

Pang, L., Sager, P., Yang, X., Shi, H., Sannajust, F., Brock, M., Wu, J.C., Abi-Gerges, N., Lyn-Cook, B., Berridge, B.R., and Stockbridge, N. (2019). Workshop report: FDA workshop on improving cardiotoxicity assessment with human-relevant platforms. Circ. Res. *125*, 855–867. https://doi.org/10.1161/CIRCRESAHA.119.315378.

Patnaik, J.L., Byers, T., DiGuiseppi, C., Dabelea, D., and Denberg, T.D. (2011). Cardiovascular disease competes with breast cancer as the leading cause of death for older females diagnosed with breast cancer: a retrospective cohort study. Breast Cancer Res. *13*, R64. https://doi.org/10.1186/bcr2901.

Perez, E.A., Koehler, M., Byrne, J., Preston, A.J., Rappold, E., and Ewer, M.S. (2008). Cardiac safety of lapatinib: pooled analysis of 3689 patients enrolled in clinical trials. Mayo Clin. Proc. *83*, 679–686. https://doi.org/10.4065/83.6.679.

Petrelli, F., Lazzari, C., Ardito, R., Borgonovo, K., Bulotta, A., Conti, B., Cabiddu, M., Capitanio, J.F., Brighenti, M., Ghilardi, M., et al. (2018). Efficacy of ALK inhibitors on NSCLC brain metastases: a systematic review and pooled analysis of 21 studies. PLoS One *13*, e0201425. https://doi.org/10.1371/journal.pone.0201425.

Porto, R., Mengarda, A.C., Cajas, R.A., Salvadori, M.C., Teixeira, F.S., Arcanjo, D.D.R., Siyadatpanah, A., Pereira, M.L., Wilairatana, P., and Moraes, J. (2021). Antiparasitic properties of cardiovascular agents against human intravascular parasite schistosoma mansoni. Pharmaceuticals (Basel) *14*, 686. https://doi.org/10.3390/ph14070686.

Qureshi, Z.P., Seoane-Vazquez, E., Rodriguez-Monguio, R., Stevenson, K.B., and Szeinbach, S.L. (2011). Market withdrawal of new molecular entities approved in the United States from 1980 to 2009. Pharmacoepidemiol. Drug Saf. *20*, 772–777. https://doi.org/10.1002/pds.2155.

Ranjan, A., Gupta, P., and Srivastava, S.K. (2016). Penfluridol: an antipsychotic agent suppresses metastatic tumor growth in triple-negative breast cancer by inhibiting integrin signaling axis. Cancer Res. *76*, 877–890. https://doi.org/10.1158/0008-5472.Can-15-1233.

Ranjan, A., and Srivastava, S.K. (2016). Penfluridol suppresses pancreatic tumor growth by autophagy-mediated apoptosis. Sci. Rep. *6*, 26165. https://doi.org/10.1038/srep26165.

Riva, E., Gerna, M., Neyroz, P., Urso, R., Bartosek, I., and Guaitani, A. (1982). Pharmacokinetics of amiodarone in rats. J. Cardiovasc. Pharmacol. *4*, 270–275. https://doi.org/10.1097/00005344-198203000-00016.

Ronaldson-Bouchard, K., and Vunjak-Novakovic, G. (2018). Organs-on-a-Chip: a fast track for engineered human tissues in drug development. Cell Stem Cell *22*, 310–324. https://doi.org/10.1016/j.stem.2018.02.011.

Sanchez-Mazas, A., Djoulah, S., Busson, M., Le Monnier de Gouville, I., Poirier, J.C., Dehay, C., Charron, D., Excoffier, L., Schneider, S., Langaney, A., et al. (2000). A linkage disequilibrium map of the MHC region based on the analysis of 14 loci haplotypes in 50 French families. Eur. J. Hum. Genet. *8*, 33–41. https://doi.org/10.1038/sj.ejhg.5200391.

Sharma, A., Burridge, P.W., McKeithan, W.L., Serrano, R., Shukla, P., Sayed, N., Churko, J.M., Kitani, T., Wu, H., Holmström, A., et al. (2017). High-throughput screening of tyrosine kinase inhibitor cardiotoxicity with human induced pluripotent stem cells. Sci. Transl Med. *9*, eaaf2584. https://doi.org/10.1126/scitranslmed.aaf2584.

Sharma, A., Sances, S., Workman, M.J., and Svendsen, C.N. (2020). Multilineage human iPSC-derived platforms for disease modeling and drug discovery. Cell Stem Cell *26*, 309–329. https://doi.org/10.1016/j.stem.2020.02.011.

Siramshetty, V.B., Nickel, J., Omieczynski, C., Gohlke, B.O., Drwal, M.N., and Preissner, R. (2016). WITHDRAWN–a resource for withdrawn and discontinued drugs. Nucleic Acids Res. *44*, D1080–D1086. https://doi.org/10.1093/nar/gkv1192.

Takahashi, K., Tanabe, K., Ohnuki, M., Narita, M., Ichisaka, T., Tomoda, K., and Yamanaka, S. (2007). Induction of pluripotent stem cells from adult human fibroblasts by defined factors. Cell *131*, 861–872. https://doi.org/10.1016/j.cell.2007.11.019.

Taylor, C.J., Peacock, S., Chaudhry, A.N., Bradley, J.A., and Bolton, E.M. (2012). Generating an iPSC bank for HLA-matched tissue transplantation based on known donor and recipient HLA types. Cell Stem Cell *11*, 147–152. https://doi.org/10.1016/j.stem.2012.07.014.

Theodoris, C.V., Zhou, P., Liu, L., Zhang, Y., Nishino, T., Huang, Y., Kostina, A., Ranade, S.S., Gifford, C.A., Uspenskiy, V., et al. (2021). Network-based screen in iPSC-derived cells reveals therapeutic candidate for heart valve disease. Science *371*, eabd0724. https://doi.org/10.1126/science.abd0724.

Tohyama, S., Hattori, F., Sano, M., Hishiki, T., Nagahata, Y., Matsuura, T., Hashimoto, H., Suzuki, T., Yamashita, H., Satoh, Y., et al. (2013). Distinct metabolic flow enables large-scale purification of mouse and human pluripotent stem cell-derived cardiomyocytes. Cell Stem Cell *12*, 127–137. https://doi.org/10.1016/j.stem.2012.09.013.

Tomlinson, B., Chan, P., and Liu, Z.-M. (2018). Statin responses in Chinese patients. J. Atheroscler. Thromb. *25*, 199–202. https://doi.org/10.5551/jat.40204.

Tuan, N.M., and Lee, C.H. (2019). Penfluridol as a candidate of drug repurposing for anticancer agent. Molecules *24*, 3659. https://doi.org/10.3390/molecules24203659.

Umekage, M., Sato, Y., and Takasu, N. (2019). Overview: an iPS cell stock at CiRA. Inflamm. Regen. *39*, 17. https://doi.org/10.1186/s41232-019-0106-0.

Van Herendael, H., and Dorian, P. (2010). Amiodarone for the treatment and prevention of ventricular fibrillation and ventricular tachycardia. Vasc. Health Risk Manag. *6*, 465–472. https://doi.org/10.2147/vhrm.s6611.

Vatine, G.D., Barrile, R., Workman, M.J., Sances, S., Barriga, B.K., Rahnama, M., Barthakur, S., Kasendra, M., Lucchesi, C., Kerns, J., et al. (2019). Human iPSC-derived blood-brain barrier chips enable disease modeling and personalized medicine applications. Cell Stem Cell *24*, 995–1005.e1006. https://doi.org/10.1016/j.stem.2019.05.011.

Warren, C.R., and Cowan, C.A. (2018). Humanity in a dish: population genetics with iPSCs. Trends Cell Biol *28*, 46–57. https://doi.org/10.1016/j.tcb.2017.09.006.

Wouters, O.J., McKee, M., and Luyten, J. (2020). Estimated research and development investment needed to bring a new medicine to market, 2009-2018. Jama *323*, 844–853. https://doi.org/10.1001/jama.2020.1166.

Xie, Q., Li, W., Huang, Z., and Zhang, Z. (2012). Effect of didrovaltrate on l-calcium current in rabbit ventricular myocytes. J. Tradit Chin Med. *32*, 442–445. https://doi.org/10.1016/s0254-6272(13)60052-7.

Zhang, S., Liu, X., Bawa-Khalfe, T., Lu, L.S., Lyu, Y.L., Liu, L.F., and Yeh, E.T. (2012). Identification of the molecular basis of doxorubicin-induced cardiotoxicity. Nat. Med. *18*, 1639–1642. https://doi.org/10.1038/nm.2919.

STAR★METHODS

KEY RESOURCES TABLE

REAGENT or RESOURCE	SOURCE	IDENTIFIER
Antibodies		
Mouse monoclonal anti-OCT4 (IgG)	Santa Cruz Biotechnology	Cat# sc5279, RRID: AB_628051
Mouse monoclonal anti-SSEA4 (IgG)	Millipore	Cat# MAB4304, RRID: AB_177629
Mouse monoclonal anti-TRA-1-60 (IgM)	Millipore	Cat# MAB4360, RRID: AB_2119183
Rabbit polyclonal anti-SOX2 (IgG)	Thermo Fisher Scientific	Cat# 481400, RRID: AB_2533841
Alexa Fluor 488 Goat polyclonal anti-mouse IgG	Thermo Fisher Scientific	Cat# A11001, RRID: AB_2534069
Alexa Fluor 488 Goat polyclonal anti-mouse IgG, IgM	Thermo Fisher Scientific	Cat# A10680, RRID: AB_2534062
Alexa Fluor 488 Goat polyclonal anti-rabbit IgG	Thermo Fisher Scientific	Cat# A11008, RRID: AB_143165
Mouse monoclonal anti-Troponin I	Santa Cruz Biotechnology	Cat# sc133117, RRID: AB_1568832
Mouse monoclonal anti-alpha-actinin	Sigma-Aldrich	Cat# A7811, RRID: AB_476766
Mouse monoclonal anti-mitochondria, surface of intact mitochondria, clone 113-1 antibody	Millipore	Cat# MAB1273, RRID: AB_94052
Alexa Fluor 568 Goat polyclonal anti-mouse IgG	Thermo Fisher Scientific	Cat# A11004, RRID: AB_2534072
Rabbit monoclonal anti-Sox2	Merck	Cat#ab5603; RRID: AB_2286686
Chicken polyclonal anti-MAP2	abcam	Cat#ab92434; RRID:AB_2138147
Mouse monoclonal [2C1.3A11] anti-Nestin	abcam	Cat#ab18102, RRID:AB_444246
Mouse monoclonal anti-Pax6	BioLegend	Cat# 862002, RRID:AB_2801238
Mouse monoclonal anti-FOX3 (NeuN)	BioLegend	Cat# 834501, RRID:AB_2564991
Goat polyclonal anti-Tyrosine Hydroxylase	Thermo Fisher Scientific	Cat# PA1-4679, RRID:AB_561880
Mouse monoclonal anti-GAD65	abcam	Cat# ab26113, RRID:AB_448989
Rabbit polyclonal anti-VGLUT1	Synaptic Systems	Cat# 135 302, RRID:AB_887877
Mouse monoclonal anti-GFAP	abcam	Cat# ab10062, RRID:AB_296804
Goat Anti-Rabbit IgG (H + L) Antibody, Alexa Fluor 568 Conjugated	Thermo Fisher Scientific	Cat# A-11011, RRID:AB_143157
Goat Anti-Chicken IgG Antibody, Alexa Fluor 647 Conjugated	Innovative Research	Cat# A21449, RRID:AB_1500594
Rabbit anti-Goat IgG (H + L) Cross-Adsorbed Secondary Antibody, Alexa Fluor 488	Thermo Fisher Scientific	Cat# A-11078, RRID:AB_2534122
Alexa Fluor(R) 647 Goat anti-mouse IgG (minimal x-reactivity) antibody	BioLegend	Cat# 405322, RRID:AB_2563045
Rabbit polyclonal anti-Connexin 43	abcam	Cat# ab11370, RRID:AB_297976
Bacterial and virus strains		
CTS™ CytoTune™-iPS 2.1 Sendai Reprogramming Kit	Thermo Fisher Scientific	Cat# A34546
Biological Samples		
Primary human PBMCs, THTC-PBMC-01	This paper	N/A
Primary human PBMCs, THTC-PBMC-02	This paper	N/A
Primary human PBMCs, THTC-PBMC-03	This paper	N/A
Primary human PBMCs, THTC-PBMC-04	This paper	N/A
Primary human PBMCs, THTC-PBMC-05	This paper	N/A
Primary human PBMCs, THTC-PBMC-06	This paper	N/A
Primary human PBMCs, THTC-PBMC-07	This paper	N/A
Primary human PBMCs, THTC-PBMC-08	This paper	N/A
Primary human PBMCs, THTC-PBMC-09	This paper	N/A
Primary human PBMCs, THTC-PBMC-10	This paper	N/A
Primary human PBMCs, THTC-PBMC-11	This paper	N/A
Primary human PBMCs, THTC-PBMC-12	This paper	N/A
Primary human PBMCs, THTC-PBMC-13	This paper	N/A
Chemicals, peptides, and recombinant proteins		

(*Continued on next page*)

Continued

REAGENT or RESOURCE	SOURCE	IDENTIFIER
TRIzol	Thermo Fisher Scientific	Cat# 15596018
H&E Staining Kit	abcam	Cat# ab245880
DAPI (4′,6-Diamidino-2-Phenylindole, Dihydrochloride)	Thermo Fisher Scientific	Cat# D1306
2375 FDA-approved compounds for cardiotoxicity evaluation	Huang et al. (2019)	N/A
2080 approved drugs for neurotoxicity evaluation	TargetMol, MA	Cat# L1000
Wheat Germ Agglutinin, Alexa Fluor 488 Conjugate	Thermo Fisher Scientific	Cat# W11261
Dimethyl sulfoxide	Sigma-Aldrich	Cat# D2650
Calcein AM	Thermo Fisher Scientific	Cat# C1430
Propidium Iodide	Millipore	Cat# P3566
Rho-associated protein kinase inhibitor (ROCK)	Selleckchem	Cat# s1049
Stemflex medium	Thermo Fisher Scientific	Cat# A3349401
DMEM F12	Thermo Fisher Scientific	Cat# 11320082
N-2 Supplement	Thermo Fisher Scientific	Cat# 17502048
Neurobasal medium	Thermo Fisher Scientific	Cat# 21103049
B-27 Supplement minus insulin	Thermo Fisher Scientific	Cat# A1895601
B-27 Supplement	Thermo Fisher Scientific	Cat# 17504-044
B-27 Supplement minus vitamin A	Thermo Fisher Scientific	Cat# 12587010
Human FGF-basic	Thermo Fisher Scientific	Cat# PHG0263
Y27632	Selleckchem	Cat# s1049
L Glutamine (200mM)	Thermo Fisher Scientific	Cat# 25-030-081
MEM Non-Essential Amino Acids Solution	Thermo Fisher Scientific	Cat# 11140-050
Heparin	Merck	Cat# H3149
2-Mercaptoethanol	Thermo Fisher Scientific	Cat# 21985023
GlutaMAX	Thermo Fisher Scientific	Cat# 35050-061
Insulin solution human, Chemically defined, recombinant, expressed in Saccharomyces cerevisiae, sterile-filtered, BioXtra, suitable for cell culture	Sigma-Aldrich	Cat# I9278
Superscript IV reverse transcriptase	Thermo Fisher Scientific	Cat# 18-090-050
CHIR99021	Selleckchem	Cat# S2924
IWR-1	Sigma-Aldrich	Cat# I0161
Hoechst 33342	Thermo Fisher Scientific	Cat# H3570
Matrigel® Growth Factor Reduced (GFR) Basement Membrane Matrix, LDEV-free	Corning	Cat# 354230
Matrigel®	Corning	Cat# 356234
Laminin Mouse Protein, Natural	Thermo Fisher Scientific	Cat# 23017015
Molecular Probes ProLong Gold Antifade Mountant	Thermo Fisher Scientific	Cat# P36930
Tissue Freezing Medium	Leica	Cat# 14020108926
Fluo-4 AM	Thermo Fisher Scientific	Cat# F-14201
Pluronic acid	Thermo Fisher Scientific	Cat# P3000MP
Critical commercial assays		
Cell Titer-Glo® Luminescent Cell Viability Assay	Promega	Cat# G7570
In Situ Cell Death Detection Kit, TMR red	Sigma-Aldrich	Cat# 12156792910
DNeasy® Blood & Tissue Kit	Qiagen	Cat# 69504
HLAssure A SBT Kits	TBG Biotechnology	Cat# 50110
HLAssure B SBT Kits	TBG Biotechnology	Cat# 50210
HLAssure C SBT Kits	TBG Biotechnology	Cat# 50410
HLAssure DRB1 SBT Kits	TBG Biotechnology	Cat# 50350
HLAssure DQB1 SBT Kits	TBG Biotechnology	Cat# 50510
HLAssure DPB1 SBT Kits	TBG Biotechnology	Cat# 50610

(*Continued on next page*)

Continued

REAGENT or RESOURCE	SOURCE	IDENTIFIER
Experimental models: Cell lines		
THTC-iPSC-01	This paper	N/A
THTC-iPSC-02	This paper	N/A
THTC-iPSC-03	This paper	N/A
THTC-iPSC-04	This paper	N/A
THTC-iPSC-05	This paper	N/A
THTC-iPSC-06	This paper	N/A
THTC-iPSC-07	This paper	N/A
THTC-iPSC-08	This paper	N/A
THTC-iPSC-09	This paper	N/A
THTC-iPSC-10	This paper	N/A
THTC-iPSC-11	This paper	N/A
THTC-iPSC-12	This paper	N/A
THTC-iPSC-13	This paper	N/A
Oligonucleotides		
Primers for Sendai virus detection, see Figure S1A SeV/181 bp F: GGATCACTAGGTGATATCGAGC/	This paper	N/A
SeV/181 bp R: ACCAGACAAGAGTTTAAGAGATATGTATC	This paper	N/A
Klf4/410 bp F: TTCCTGCATGCCAGAGGAGCCC	This paper	N/A
Klf4/410 bp R: AATGTATCGAAGGTGCTCAA	This paper	N/A
KOS/528 bp F: ATGCACCGCTACGACGTGAGCGC	This paper	N/A
KOS/528 bp R: ACCTTGACAATCCTGATGTGG	This paper	N/A
c-Myc/532 bp F: TAACTGACTAGCAGGCTTGTCG/	This paper	N/A
c-Myc/532 bp R: TCCACATACAGTCCTGGATGATGATG	This paper	N/A
House-Keeping Gene, used in Figure S1A GAPDH/302 bp F: AGCCACATCGCTCAGACACC/	This paper	N/A
GAPDH/302 bp R: GTACTCAGCGGCCAGCATCG	This paper	N/A
Software and algorithms		
AccuType HLA SBT Analysis Software	TBG Biotechnology	http://www.tbgbio.com/en/product/product_detail/48
CellProfiler	Carpenter et al. (2006)	https://cellprofiler.org
Graphpad Prism	Graphpad	https://www.graphpad.com
Affinity Designer	Affinity	https://affinity.serif.com

RESOURCE AVAILABILITY

Lead contact

Further information and requests for resources and reagents should be directed to and will be fulfilled by the Lead Contact Patrick C. H. Hsieh (phsieh@ibms.sinica.edu.tw).

Materials availability

All materials generated in this study are available upon request from the Lead Contact and upon signature of the corresponding Material Transfer Agreement, if necessary.

Data and code availability

- All data reported in this paper will be shared by the lead contact upon request.
- This paper does not report original code.
- Any additional information required to reanalyze the data reported in this paper is available from the lead contact upon request.

EXPERIMENTAL MODEL AND SUBJECT DETAILS

Human donors

Institutional permission and oversight of human sample handling was approved by Academia Sinica (AS-IRB-BM-170120 v.3). The sample size of 1000 donors was estimated based on the frequency of HLA alleles in Taiwan previously reported by Lai et al. (2010). Blood was drawn from 13 healthy individuals to generate iPSCs based on their HLA homozygosity. The mean donor age was 46.4 years old (SD 11.6 years). There were 5 males and 8 females included in the study. Refer to Table S1 for cell line-specific donor information.

Mice

All animal experiments were conducted in accordance with the Guide for the Use and Care of Laboratory Animals (ARRIVE guidelines). Mice (C57BL/6 and NOD/SCID) were purchased from the National Laboratory Animal Center, Taiwan. For teratoma formation and engraftment studies, 12 week old male NOD/SCID mice were used. For *in vivo* toxicity assays, 8 week old male C57BL/6 mice were used. All animals were housed under standard laboratory conditions in the animal core facility at Academia Sinica and all study protocols were approved by the Academia Sinica Institutional Animal Care and Utilization Committee in accordance with IACUC guidelines.

METHOD DETAILS

Donor recruitment

The study was approved by the Institutional Review Board of Biomedical Science Research at Academia Sinica (approval number: AS-IRB-BM-170120 v.3). The individuals in this study signed written informed consent to donate PBMCs for HLA genotyping and iPSC generation.

HLA typing

We recruited 1,000 healthy donors and performed HLA PCR sequencing-based typing (PCR-SBT) for HLA genotyping. As the HLA-B locus is the most polymorphic, our strategy was to first focus on genotyping donors' HLA-B locus. Once HLA-B homozygous donors were identified, they were rescreened for the remaining HLA genotypes. Whole blood (5 mL) was collected into acid citrate tubes (BD), and the genomic DNA was isolated using the DNeasy® Blood & Tissue Kit (Qiagen). HLA-typing was performed using the PCR-SBT method. HLA genotyping was carried out using HLAssure A, B, C, DQB1, DRB1 & DPB1 SBT Kits (TBG Biotechnology) on ABI 3730XL DNA Analyzers (Applied Biosystems) with AccuType HLA SBT Analysis Software (TBG Biotechnology) as described in the manufacturer's protocol. As parents' samples were not available, the haplotypes were not obtained by segregation.

Global HLA haplotype frequencies and population coverage

The global haplotype frequencies of HLA-A*33:03-B*58:01-DRB1*03:01, HLA-A*02:07-B*46:01-DRB1*09:01, HLA-A*02:07-B*46:01-DRB1*08:03, HLA-A*02:01-B*40:01-DRB1*11:01, HLA-A*11:01-B*13:01-DRB1*16:02, and HLA-A*11:01-B*39:01-DRB1*08:03 were calculated by combining haplotype information from 3,219,526 individuals collected by 89 HLA studies obtained from the Allele Frequency Net Database (http://www.allelefrequencies.net/ (Gonzalez-Galarza et al., 2020)). The inclusion of allele-specific data depended on whether data at the level of HLA protein (i.e., HLA-B 58:01) was available and when the sample size was greater than 100. Population haplotype frequency data were consolidated by country as a mean of all sub-population haplotype frequencies obtained from the database. The global population coverage in terms of the numbers of the HLA haplotype carriers were aggregated by country as the mean of all constituent population haplotype frequencies weighted by each country's population in 2021 as reported on each government's official website.

Detection of sendai virus expression

To ensure hiPSCs are Sendai virus and transgenes free, total RNA was extracted from > passage 10 cells using TRIzol reagent (Thermo Fisher Scientific). Then, reverse transcription was performed by Superscript IV reverse transcriptase (Thermo Fisher Scientific). The primer sequences and PCR reaction were designed and performed as recommended by the manufacturer (Thermo Fisher Scientific). Primer details are listed in Table S7.

Immunocytochemistry

Immunocytochemistry was performed as previously described (Huang et al., 2020). Briefly, cells were fixed in 4% paraformaldehyde, and then permeabilized using 0.1% Triton X-100 when required. Specific primary antibodies were incubated overnight.

Subsequently, appropriate Alexa 594, Alexa 488, and Alexa 647-conjugated secondary antibodies (Molecular Probes) were incubated for 1 h at room temperature. Imaging was captured using a Zeiss LSM 700 confocal microscope (Carl Zeiss) and processed through Zen imaging software.

Teratoma formation assay

A million hiPSCs were resuspended in 50% Matrigel (Corning) and then injected into the testis of 12 week old NOD/SCID mice (National Laboratory Animal Center (NLAC), Taiwan). Mice were sacrificed at 6 weeks after transplantation. The teratomas were fixed and embedded in paraffin for serial sectioning and histological analysis by haemotoxylin and eosin staining to confirm differentiation potential into different germ layers.

Karyotyping analysis

To examine the genetic stability of representative iPSCs, cells were treated with 10 μg/mL of colcemid for 20 min at 37°C to induce cell-cycle arrest and then incubated with 75 mM hypotonic KCl to obtain nuclear swelling. The cells were then fixed with 3:1 methanol/glacial acetic acid. Metaphase chromosomes were harvested and subjected to Giemsa staining for cytogenic analysis of G-bands (20 metaphase spreads were counted).

Compound collections

A proprietary collection of 2,374 approved and pharmacopoeia drugs (Huang et al., 2019) was applied for cardiotoxicity evaluation. Neurotoxicity was assessed by a compound library containing 2080 approved drugs (TargetMol, MA). These drugs were dissolved in DMSO and arrayed at a concentration of 1 mM in 1536-well and 384-well microtiter plates before application. Addition of drug to assay plates was conducted by a pin-tool transferring station equipped in the ultra-High-Throughput Screening System (uHTS) of the Genomics Research Center, Academia Sinica. The final assay concentration of the drugs was designed and controlled by the slotted open/volume of the pin (V&P Scientific, CA), which provides accurate and precise delivery of liquid at a coefficient of variation (CV) average under 5%.

Human iPSC generation

Blood samples were collected into BD Vacutainer® cell preparation tubes for the separation of mononuclear cells according to the manufacturer's instructions. Cells were then reprogrammed through CytoTune-iPS 2.0 Sendai Reprogramming Kit (Thermo Fisher Scientific).

Cardiac differentiation

HiPSCs were differentiated as previously described (Huang et al., 2019). In brief, hiPSCs were seeded on a Matrigel-coated plate. Once cells reached ~80% confluency, they were treated with 6–10 μM CHIR99021 (Selleckchem) to activate Wnt signaling to induce mesoderm differentiation. Then, the medium was refreshed to RPMI/B27 insulin-free medium (Thermo Fisher Scientific) at day 2. At day 3, cells were then treated with 5 μM IWR-1 (Sigma) for a further 48 h. After two days, the medium was changed to remove IWR-1. Cells were then cultured in RPMI/B27 medium until cells started to beat. Cells were then cultured in glucose-free RPMI/B27 for purification.

Cell culture and compound treatment for cardiotoxicity screening

Forty-four day hiPSC-CMs were plated in black clear-bottom Matrigel-coated, 1536-well plates (PerkinElmer) at 800 cells per well using an automatic dispenser (GNF Systems). After incubation for 3 days, hiPSC-CMs were treated for 24 h with a final concentration of 100 μM compounds or DMSO (10%). Doxorubicin (30 μM) was used as a reference compound and a DMSO vehicle-treated group was used as a negative control. Cells were then co-stained with Hoechst 33342 (Thermo Fisher Scientific), for total nuclei count, and propidium iodide, to detect dead cells. Wells were imaged using Opera Phenix™ High-Content Screening System (PerkinElmer) using a whole-well imaging method to quantify live/dead percentage. Doxorubicin (30 μM) was used as positive control in each batch of the screenings. Initially, potent drugs that induced >80% cardiotoxicity in more than 3 cell lines were selected as hits for validation. The selected hits were Pyrvinium (Selleckchem), Topotecan (Selleckchem), Didrovaltrate (ChemFaces), Doxorubicin (TargetMol), Valtrate (TargetMol), Doxycycline (Selleckchem), Daunorubicin (Selleckchem), Lapatinib (Selleckchem), Yohimbine (Sigma), Pararosaniline (Sigma), Demeclocycline (TargetMol), Cetrorelix (TargetMol), Meclocycline sulfosalicylate (Sigma), Idarubicin (TargetMol) and Ethacridine lactate (TargetMol). An 8-point dilution assay (0.6 μM, 1 μM, 3 μM, 6 μM, 10 μM, 30 μM, 60 μM, and 100 μM) was conducted in triplicate to generate dose-response curves. The assay protocol was the same as that of the initial drug screening described above. Cell viability was detected using CellTiter-Glo® Luminescent Cell Viability Assay (Promega) and imaged by the ViewLux plate reader (PerkinElmer).

Fabrication of a multi-well plate with embedded microgrooves

A silicon wafer was first cleaned using Piranha solution followed by buffered oxide etching. Then a layer of 4 μm thick SU-8 2005 photoresist was spun coated on the silicon wafer followed by the standard SU-8 photolithography process. Multiple SU-8 concentric microgrooves with 20 μm separation and 4 μm depth were created. Then, the inverse pattern of microgrooves was transferred to a 0.3 mm thick polypropylene (PP) sheet using the hot embossing process. The molding temperature, pressure, and dwell time were controlled to create round edges on PP microgrooves. Then, this PP master was peeled off from the SU-8 master. A PMMA open

bottom multi-well plate was attached to this PP master that had 48 patterns of microgrooves. Room-temperature-vulcanizing (RTV) silicone was poured in the PMMA multi-well plate to create an RTV microgroove-stamp. After RTV stamps were cured, they were taken out of the PMMA multi-well plate. Then, a thin layer of polydimethylsiloxane (PDMS) monomer and curing agent (Sylgard 184) mix was applied on the surface of the RTV stamps, and 96 of these stamps were put inside the wells of a standard CellCarrier-96 Ultra microplate (PerkinElmer). After curing in a 55°C oven, RTV stamps were pulled out from each well and a 96-well plate with embedded microgrooves was created.

HiPSC-CM engraftment

HiPSC-CMs (day 16) were plated onto Matrigel-coated 6-well plates. Four days after plating, hiPSC-CMs were dissociated by trypsin and suspended at a density of 1×10^6 cells in 30 μL chilled injection medium (700 μL FBS, 300 μL Matrigel, containing 10 μM Caspase inhibitor Z-VAD-FMK (Calbiochem, 627610-1MGCN), 50 nM TAT-BH4/BCL-XL (Calbiochem, 197217-1MGCN), 200 nM Cyclosporine A (Sigma, P154-100MG), 50 μM Pinacidil (Sigma, 30024-25MG), 100 ng/mL IGF-1 (Peprotech, 100-11), 100 ng/mL PDGF-BB (Prprotech,100-14B), 100 ng/mL VEGF (Prprotech, 100-20). Cells were injected (10 μL) into 3 different sites on the heart wall of 12-week-old NOD-SCID mice (NLAC, Taiwan). Mice were sacrificed 3 weeks after injection. Whole hearts were harvested, treated with 4% paraformaldehyde in PBS overnight at 4°C, and dehydrated with 70% ethanol for 1 h. Samples were then paraffin-embedded and sectioned into 5 μm slices.

Micro electro array

The protocol for evaluating the effect of drugs on hiPSC-CM electrophysiology using Maestro Edge (Axion BioSystem) was as described by Axion BioSystems. The effects of drugs on cardiomyocyte electrophysiology were performed at day 47 of differentiation and recorded using the Maestro Edge. Day 33 hiPSC-CMs were plated on 50 mg/mL fibronectin-coated 24-well CytoView MEA plates (Axion BioSystems) at a density of 4×10^4 cells per well 14 days before the assay. Cells were incubated with various concentrations (ranging from 3 nM to 300 nM) of either valtrate or pyrvinium for 30 min. The effects of drugs on cardiomyocyte electrophysiology were performed at day 47 of differentiation, and recorded using the Maestro Edge (Axion BioSystem).

To assess the effect of drugs on hiPSC-NEUR, Axion Maestro 24-well microelectrode array plates were coated with poly-L-ornithine (0.1 mg/mL). HiPSC-NEUR were resuspended at a concentration of 1.2×10^7 cells/mL in Neurobasal with laminin (20 μg/mL). A 10 μL drop was added to the center of each well and cultured for 4 h after which 0.5 mL of Neurobasal Medium was added. Half the Neurobasal media was changed every 2 days for 20 days. Baseline recordings were acquired for 15 min prior to drug application using the Maestro Edge Multielectrode Array system (Axion Biosystems), then 15 min recordings were acquired 30 min following drug application.

In vivo cardiotoxicity assay

C57BL/6 mice (8-week-old; NLAC, Taiwan) were exposed to either a single intraperitoneal injection of valtrate (45 mg/kg) (Braun et al., 1984) for a day or pyrvinium (0.85 mg/kg) (Momtazi-Borojeni et al., 2018) for 3 days to induce cardiotoxicity. Cardiac function was evaluated through echography before and after drug delivery. Heart tissue was harvested after mice were sacrificed and tissue was fixed in 4% paraformaldehyde and then embedded in paraffin for serial sectioning. Cell toxicity was assessed by the In Situ Cell Death Detection Kit (Sigma) to detect apoptotic cells after drug treatment following the manufacturer's protocol.

Neuronal differentiation

To obtain neuronal stem cells (hiPSC-NSC), hiPSCs were plated in StemFlex Medium on Matrigel coated 6 well plates. The following day, media was replaced with Neuronal Induction Medium [Neurobasal medium (Thermo Fisher Scientific), 2% Neuronal Induction Supplement (Thermo Fisher Scientific)]. Cells were cultured for 7 days, then cultured in Neuronal Expansion Medium (50% Neurobasal medium, 50% DMEM/F:12 (Thermo Fisher Scientific), 2% Neuronal Induction Supplement) for a further 7 days. To generate neurons, hiPSC-NSC were plated onto poly-L-ornithine (0.1 mg/mL) and laminin (10 μg/mL) coated 6 well plates in StemPro Medium (Knockout DMEM/F:12 (Thermo Fisher Scientific), 2% StemPro Neuronal Supplement (Thermo Fisher Scientific), L-Glutamine, 10 μg/mL bFGF, 10 μg/mL EGF) for 2 days. Media was changed to Neurobasal Medium (Neurobasal Medium, 2% B27 (Gibco), L-Glutamine) for a further 21 days with half the media changed every 3 days.

Cerebral organoid generation

Cerebral organoids were generated according to a previously published protocol (Lancaster and Knoblich, 2014). In brief, on day 0, 4,500 human iPSCs were plated in each well of an ultra-low binding 96 well plates in StemFlex Medium containing 4ng/mL basic fibroblast growth factor (Thermo Fisher Scientific) and 50 μM Rho-associated protein kinase inhibitor (Selleckchem). Media was changed every other day for 6 days, then transferred to low adhesion 24 well plates in neural induction media (DMEM/F12, 1:100 N2 supplement (Thermo Fischer Scientific), Glutamax, MEM-NEAA, and 1 μg/mL heparin (Merck). Media was changed every other day for 5 days. On day 11, embryoid bodies were transferred to droplets of Matrigel and cultured in differentiation medium containing 1:1 mixture of DMEM/F12 and Neurobasal, 1:200 N2 supplement, 1:100 B27 supplement without vitamin A (Thermo Fisher Scientific), 3.5 μL/L 2-mercaptoethanol (Thermo Fisher Scientific), 1:4000 insulin (Sigma), 1:100 Glutamax, and 1:200 MEM-NEAA. After 4 days of stationary growth, plates were placed on a rotating platform with the same media as above except B27 supplement with vitamin A was used. Cells were cultured for 90 days with media changes every 2 days.

Cell culture and compound treatment for neurotoxicity screening

Forty-two day hiPSC-NEUR were plated in black, clear-bottom, poly-L ornithine-coated 1536-well plates (PerkinElmer) at 2000 cells per well using an automatic dispenser (GNF Systems). Cells were plated in neurobasal media (Thermo Fisher Scientific) containing B27 (Thermo Fisher Scientific), L-glutamine (Gibco) and laminin (10 μg/mL; Thermo Fisher Scientific). After incubation for 3 days, hiPSC-NEURs were treated for 24 h with a final concentration of 10 μM compounds or 1% DMSO. DMSO (1%) was used as a negative control and staurosporine (10 μM) was used as a positive control. The Z-factor was calculated for each plate to determine the validity of the assay. The Z-factor for the assay was calculated using the positive and negative controls and was required to be between 0.5 and 1. This was calculated using GraphPad Prism. Cell viability was detected using CellTiter-Glo® Luminescent Cell Viability Assay (Promega) and imaged using ViewLux plate reader (PerkinElmer). For the primary screen hits, the median CellTiter Glo value (luminescence value) of each plate was calculated. All compounds were normalized to this value. The 15 compounds (1% of the plate) with the lowest luminescence values were considered to be the most toxic on that plate. To be selected for further validation, the drug was required to be in the 1% list in more than 3 cell lines. An 8-point two-fold dilution assay, starting from 10 μM, was conducted in triplicate as hit reconfirmation. The same assay protocol as described above was performed for cell viability. To detect the differences in intra-donor and inter-donor variability, the IC50 for each clone was compared by one-way ANOVA using GraphPad Prism.

Dendrite analysis for neurotoxicity screening

A CellProfiler (Carpenter et al., 2006) pipeline was developed to analyze neurite morphology. Neurites were enhanced by EnhanceEdges and EnhanceOrSuppressFeatures modules, major and minor axis length were measured by the MeasureObjectSizeShape module. Neurites were then skeletonized by ConvertObjectsToImage and Morph module before measured neurite length and number of branches for individual neurons with the MeasureObjectSkeleton module.

In vivo neurotoxicity assay

C57BL/6 mice (8-week-old; NLAC, Taiwan) were exposed to daily administration by oral gavage of amiodarone (100 mg/kg) (Le Bouter et al., 2004; Porto et al., 2021) or penfluridol (60 mg/kg) (Liu et al., 2021) for 11 days to investigate neurotoxicity. Whole brains were harvested after mice were sacrificed and tissue was fixed in 4% paraformaldehyde and then frozen in Tissue Freezing Medium (Leica) for serial sagittal sectioning. Cell toxicity was assessed by the In Situ Cell Death Detection Kit (Sigma) to detect apoptotic cells after drug treatment following the manufacturer's protocol.

In vivo neuronal differentiation

HiPSC-NSCs were suspended in DMEM at a concentration of 5×10^4 cells/μL. Following craniotomy, 2 μL (1×10^5 cells) were engrafted into the right subventricular zone of 8-week-old NOD/SCID mice (NLAC, Taiwan). The coordinates for injection were as follows: anterior-posterior +0.6 mm, mediolateral +1.2 mm, dorsoventral - 3 mm from skull surface. Following engraftment for 6 weeks, whole brains were harvested and treated with 4% paraformaldehyde in PBS overnight in 4°C. Samples were then cryosectioned into 25 μm slices.

Electrophysiology

Human iPSC-NEURs were plated onto poly-L-ornithine and laminin coated glass coverslips (6×10^4 cells per coverslip) for 20 days in Neurobasal medium. On the day of experimentation, coverslips were immersed in artificial cerebrospinal fluid (ACSF; 119 mM NaCl, 2.5 mM KCl, 1.3 mM MgSO4, 26.2 mM NaHCO3, 1 mM NaH2PO4, 2.5 mM $CaCl_2$, 11 mM glucose, pH 7.4 by gassing with 5% CO_2/95% O_2). Slides were kept in the recording chamber on an upright microscope (BX51W1; Olympus Optical). Excitatory postsynaptic potentials were recorded using a glass pipette filled with intracellular solution containing 131 mM K-gluconate, 8 mM NaCl, 20 mM KCl, 10 mM HEPES, 2 mM EGTA, 2 mM Mg-ATP, 0.3 mM Na3GTP with resistance between 3 and 5 MOhm. Data were recorded with an Axon Axopatch 200B amplifier (Molecular Devices) and Digidata 1440A system (Molecular Devices) at room temperature (24–25°C). EPSC voltage clamp held at −70 mV. Data were analyzed using the pCLAMP software.

Live-cell calcium imaging

hiPSC-NEUR (1×10^5 cells) were plated onto poly-L-ornithine (0.1 mg/mL) and laminin (10 μg/mL) coated glass-bottom confocal dishes (SPL Life Sciences) in Neurobasal medium. Cells were cultured for 20 days, with half the media changed every 3 days. Cells were then washed twice with recording buffer (10 mM HEPES pH 7.35, 156 mM NaCl, 3 mM KCl, 1.25 mM KH_2PO_4, 10 mM D-glucose, 2 mM $CaCl_2$). Cells were incubated with 1 mL recording buffer containing 5 μM Fluo-4 AM (Life Technologies) and 0.0025% Pluronic acid (Thermo Fischer Scientific) for 30 min at 37°C. This was aspirated and washed twice with the recording buffer. The culture dishes were then transferred to a Carl Zeiss 880 confocal microscope where calcium responses were recorded using the ZEN 2.1 SP2 software (version 13.0.0.518). Cells were maintained at 37°C using a heated stage where images were acquired every 0.2 s for 5 min.

Statistical analysis

The data are presented as mean ± standard error of the mean. Multiple comparisons were analyzed by ANOVA followed by Bonferroni post hoc analysis, while two groups were analyzed by unpaired two-tailed Student's t-test with Graphpad Prism software (version 9.1.1). A p value of less than 0.05 was considered statistically significant.

Cell Reports, Volume *39*

Supplemental information

Population-based high-throughput toxicity screen of human iPSC-derived cardiomyocytes and neurons

Ching Ying Huang, Martin W. Nicholson, Jyun Yuan Wang, Chien Yu Ting, Ming Heng Tsai, Yu Che Cheng, Chun Lin Liu, Darien Z.H. Chan, Yi Chan Lee, Ching Chuan Hsu, Yu Hung Hsu, Chiou Fong Yang, Cindy M.C. Chang, Shu Chian Ruan, Po Ju Lin, Jen Hao Lin, Li Lun Chen, Marvin L. Hsieh, Yuan Yuan Cheng, Wan Tseng Hsu, Yi Ling Lin, Chien Hsiun Chen, Yu Hsiang Hsu, Ying Ta Wu, Timothy A. Hacker, Joseph C. Wu, Timothy J. Kamp, and Patrick C.H. Hsieh

Supplementary Information

- **Supplementary Figures S1-S6**
- **Supplementary Tables S1-S7**

SUPPLEMENTAL FIGURES

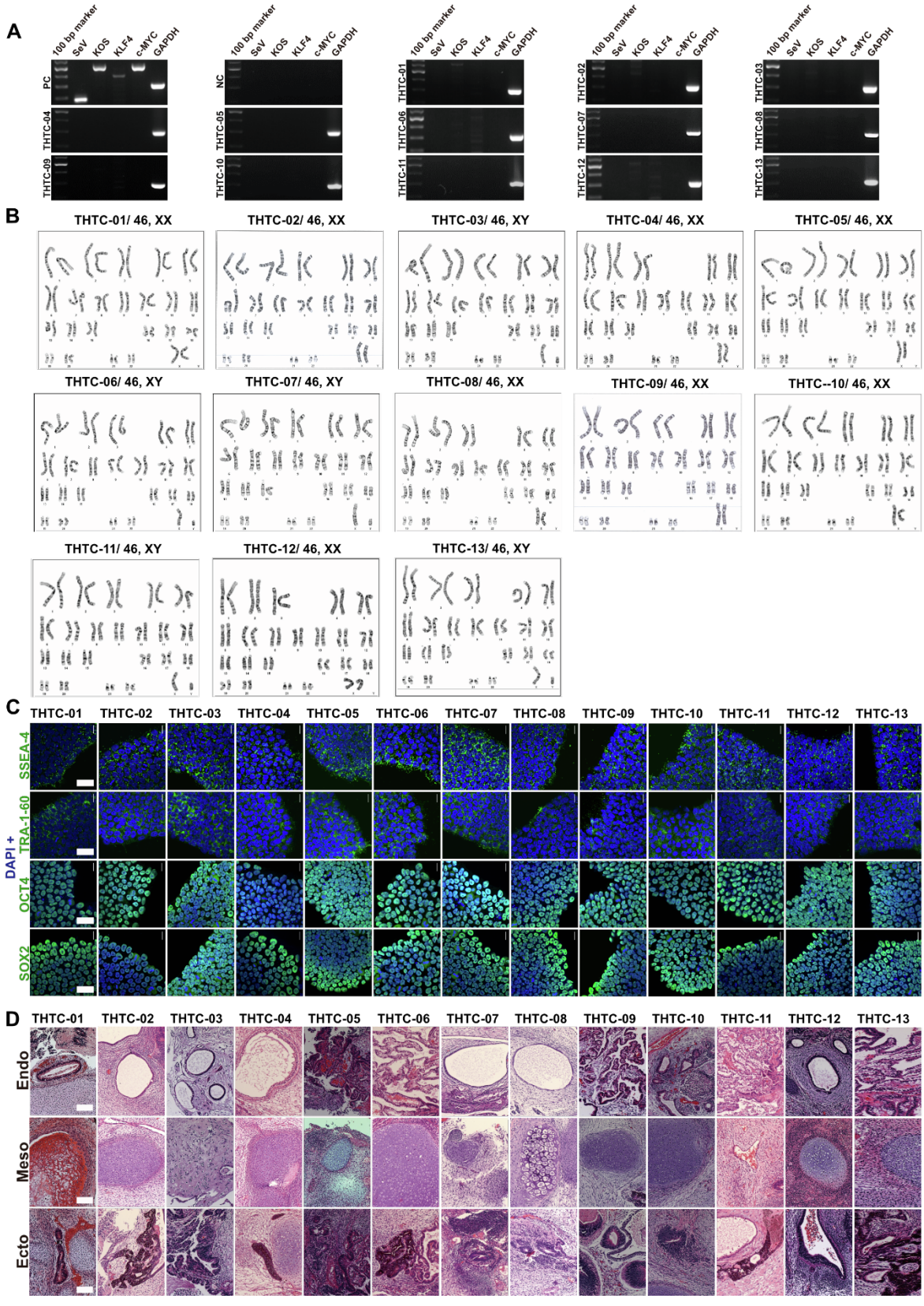

Figure S1. Characterization of HLA-homozygous hiPSC lines, related to Figure 1

(A) Analysis of Sendai virus expression in all representative HLA-homozygous hiPSC lines. RT-PCR of hiPSC lines was performed to evaluate the expression of Sendai virus (SeV), KOS (KLF4, OCT3/4, SOX-2) and c-MYC. PC; positive control (early passages of iPSC), NC; negative control.

(B) Karyotyping images of chromosomes from HLA-homozygous hiPSC lines.

(C) Immunolabeling of DAPI (blue) and various pluripotent markers SOX2, OCT4, TRA-1-60, and SSEA-4 (green). Scale bar: 40 μm.

(D) H&E staining of ectoderm (Ecto), mesoderm (Meso), and endoderm (Endo) following teratoma formation. Scale bar: 200 μM.

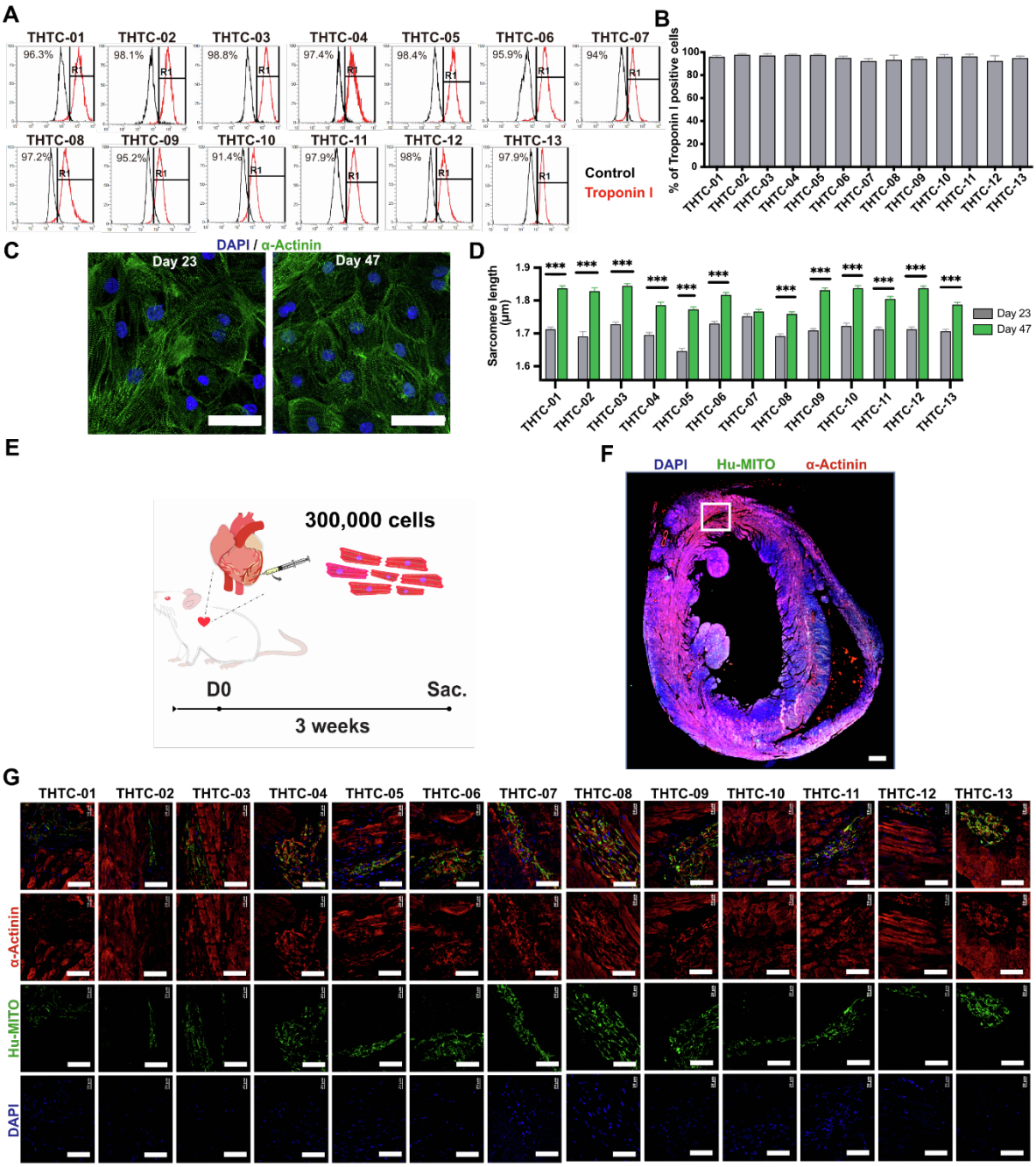

Figure S2. Characterization of cardiomyocytes, related to Figure 2

(A) Flow cytometry of cardiomyocytes after 20 days of differentiation.

(B) Bar graph showing percentage of troponin I positive cells. Bars represent mean + SEM.

(C) Immunolabeling of α–actinin (green) at day 23 and 47 cardiomyocytes. Scale bar: 60 µm.

(D) Bar graph showing the sarcomere length in cardiomyocytes at days 23 and 47. Data represent mean ± SEM. Statistical analysis performed using the unpaired t-test (***, $p < 0.001$).

(E) Diagram of injection site of cardiomyocytes.

(F) Immunolabeling of DAPI (blue), α-actinin (red) and human mitochondria (Hu-MITO; green) with (G) magnified images for each line. Scale bar in F: 450 µm. Scale bar in G: 40 µm.

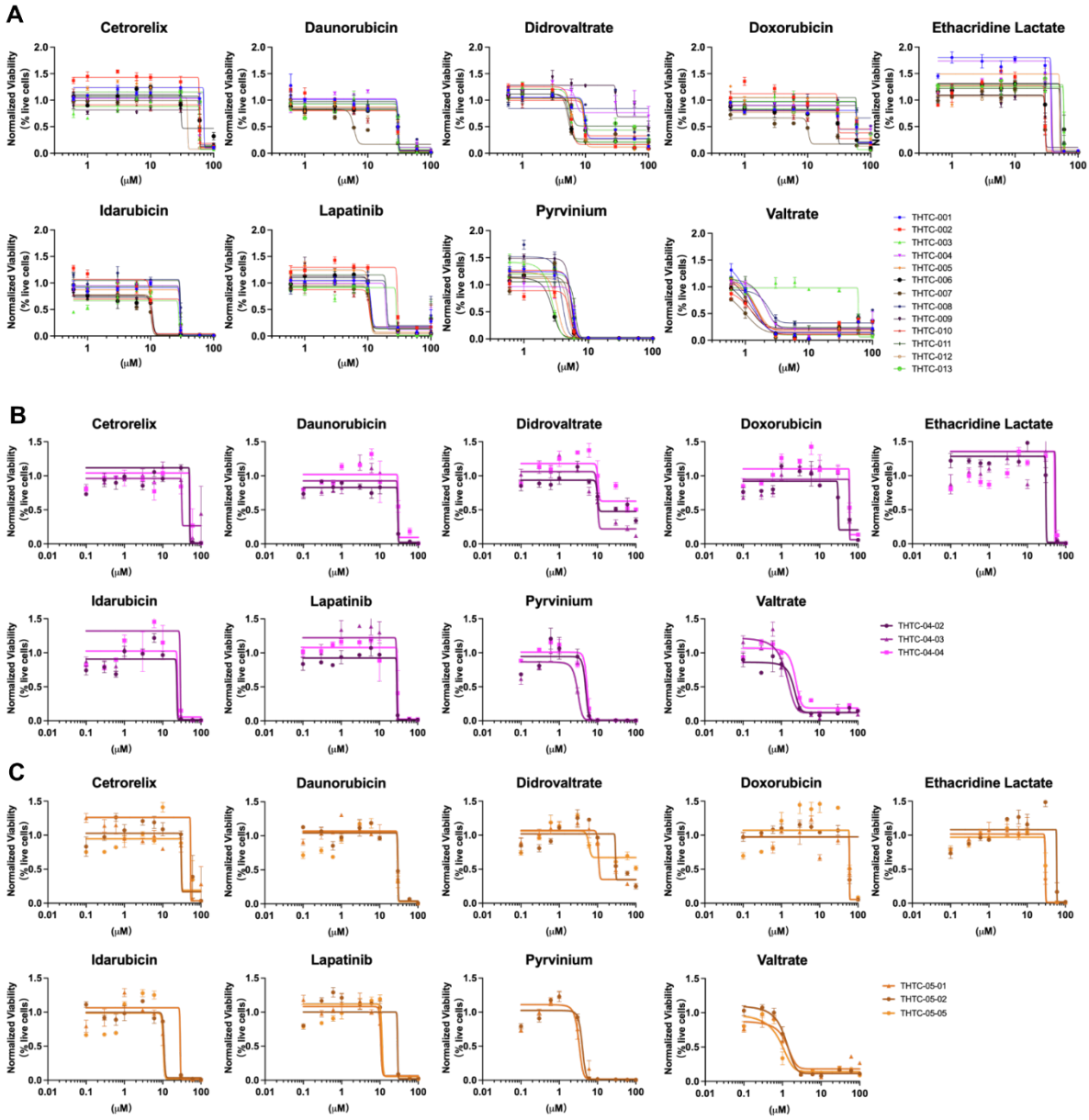

Figure S3. Hit compound validation of cardiotoxicity, related to Figure 3

(A) Comparative evaluation of cell viability by CellTiter-Glo assay of 13 HLA-homozygous hiPSC lines following 24-hour exposure to hit compounds. n = 3 for each drug concentration. Data represent mean ± SEM.

(B-C) Intra-donor variability evaluation by CellTiter-Glo assay in (B) THTC-04 and (C) THTC-05 cell lines.

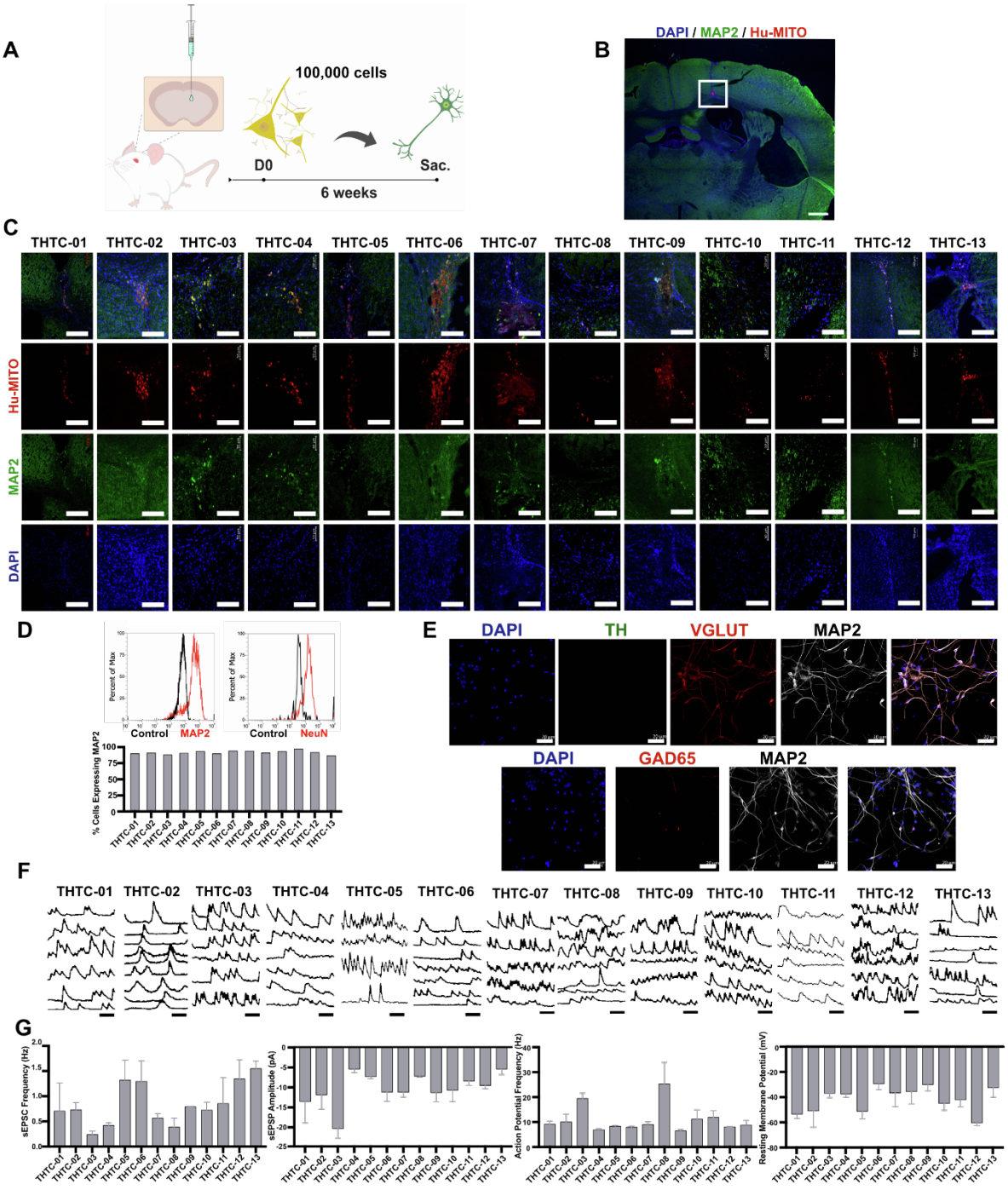

Figure S4. Human iPSC-derived neurons express mature neuronal markers and have spontaneous activity, related to Figure 4

(A) Schematic diagram of experimental design showing location of engraftment in a coronal section of mouse brain.

(B) Immunolabeling of MAP2 (green) and human mitochondria (Hu-MITO, red) and

(C) Magnified images for each cell line. Scale bar in B: 500 µm. Scale bar in G: 75 µm.

(D) Representative example of flow cytometry data of MAP2 and NeuN and quantification of cells expressing MAP2 by flow cytometry.

(E) Immunolabeling of dopaminergic neurons (TH; green), glutamatergic neurons (VGLUT; red) and MAP2 (white). In the lower panel, GABAergic neurons (GAD65; red) and MAP2 (white). Scale bar: 40 µm.
(F) Live cell calcium imaging of neurons. Scale bar: 60 seconds.
(G) Quantification of spontaneous excitatory post-synaptic potential (sEPSP) amplitude, sEPSC frequency, induced actin potential frequency, and resting membrane potential. Bars represent mean ± SEM.

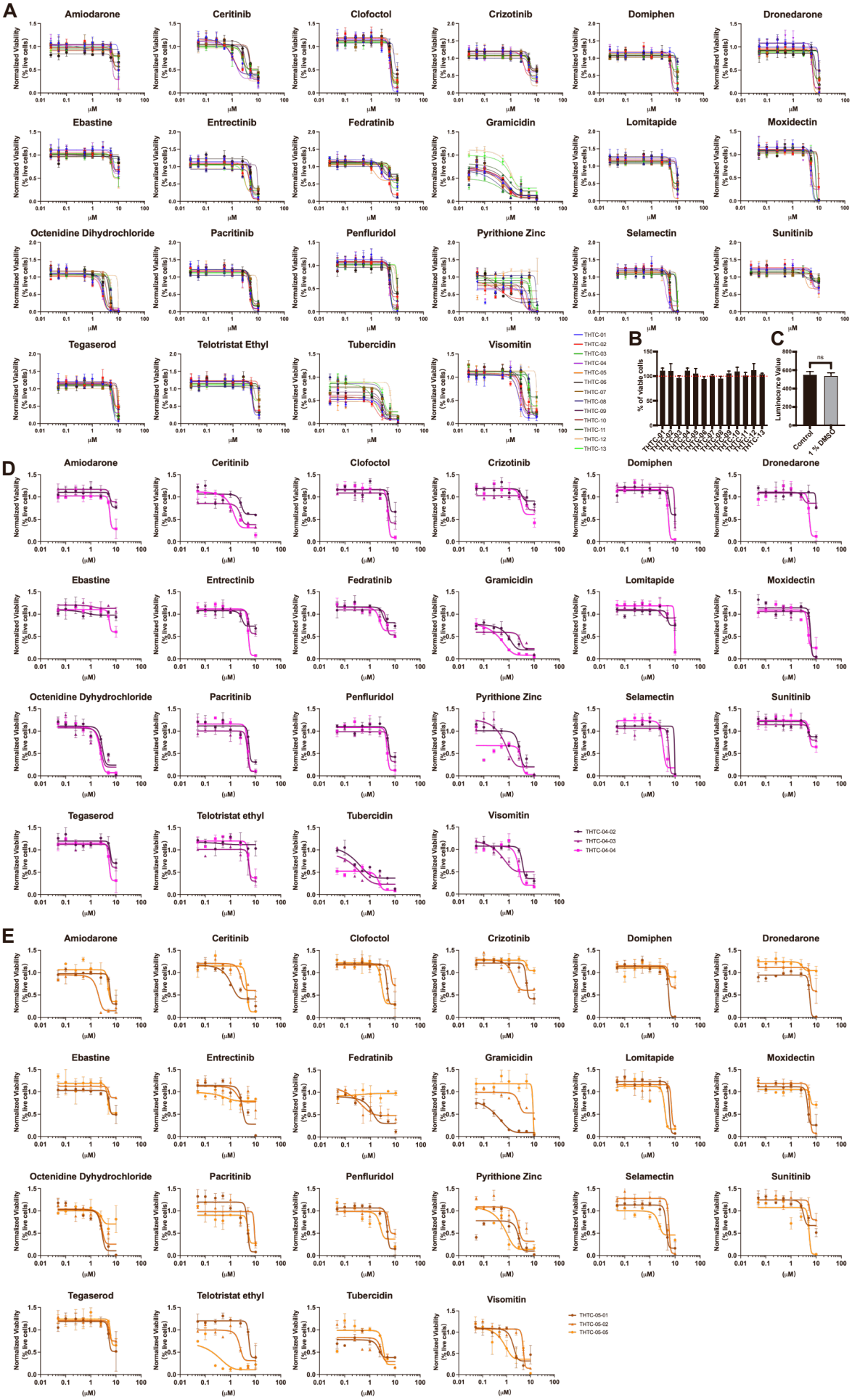
A
Amiodarone
Ceritinib
Clofoctol
Crizotinib
Domiphen
Dronedarone
Ebastine
Entrectinib
Fedratinib
Gramicidin
Lomitapide
Moxidectin
Octenidine Dihydrochloride
Pacritinib
Penfluridol
Pyrithione Zinc
Selamectin
Sunitinib
Tegaserod
Telotristat Ethyl
Tubercidin
Visomitin
Normalized Viability (% live cells)
μM
THTC-01
THTC-02
THTC-03
THTC-04
THTC-05
THTC-06
THTC-07
THTC-08
THTC-09
THTC-10
THTC-11
THTC-12
THTC-13
B
% of viable cells
C
Luminescence Value
ns
Control
1 % DMSO
D
Telotristat ethyl
(μM)
THTC-04-02
THTC-04-03
THTC-04-04
E
THTC-05-01
THTC-05-02
THTC-05-05

Figure S5. Hit compound reconfirmation of neurotoxicity, related to Figure 5

(A) Comparative evaluation of cell viability by CellTiter-Glo assay of 13 HLA-homozygous hiPSC lines following 24-hour exposure of hit compounds. n = 3 for each drug concentration.

(B) Quantification of cell viability of 1% DMSO treated cells following CellTiter-Glo assay.

(C) Quantification of the affect of 1% DMSO compared to untreated control following CellTiter-Glo assay. Student-t test, n = 13.

All data represent mean ± SEM.

(D-E) Intra-donor variability evaluation by CellTiter-Glo assay in (D) THTC-04 and (E) THTC-05 cell lines.

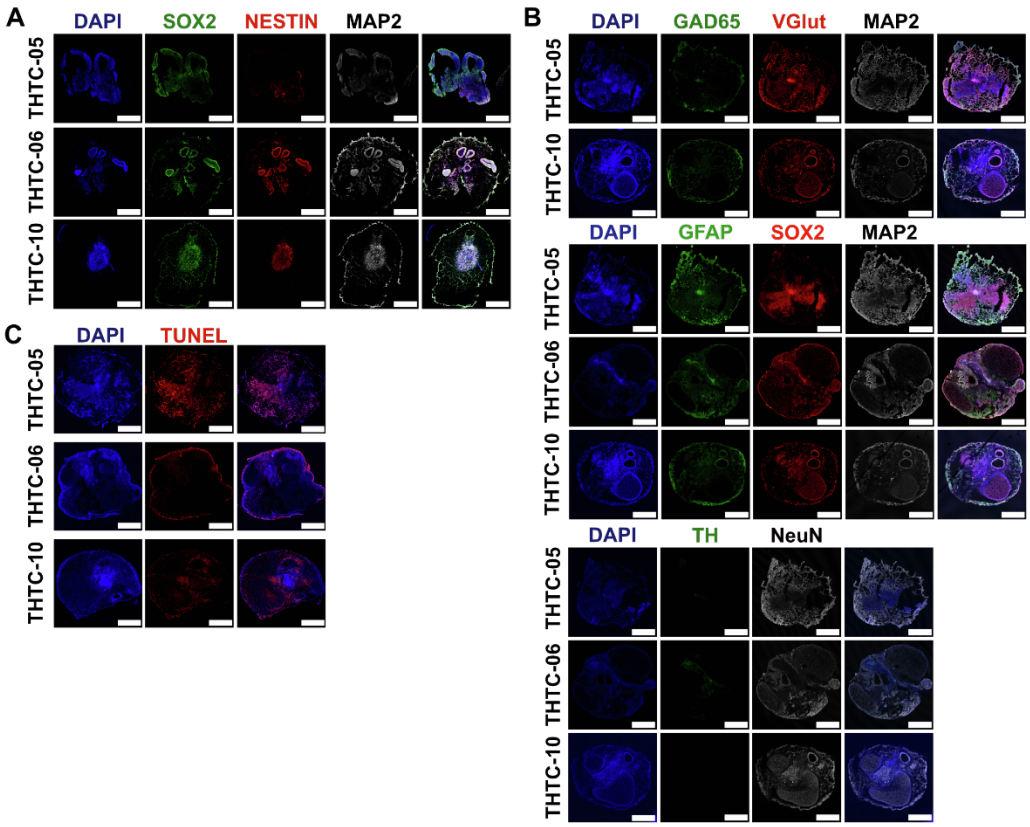

Figure S6. hiPSC-derived cerebral organoids express diverse neuronal subtypes, related to Figure 6

(A) Immunolabeling of SOX2 (green) nestin (red), and MAP2 (white) expression in day 30 cerebral organoids.

(B) Immunolabeling of day 90 cerebral organoids. Upper panel: GABAergic neurons (GAD65; green), glutamatergic neurons (VGlut; red), MAP2 (white). Middle panel: astrocytes (GFAP; green), SOX2, and MAP2 (white). Lower panel: dopaminergic neurons (TH: green) and NeuN (white).

(C) Confocal images of day 90 organoids labeled with TUNEL.

SUPPLEMENTARY TABLES

Table S1. HLA haplotypes of HLA-homozygous iPSCs, related to Figure 1.

Cell line	HLA_A		HLA_B		HLA_C		HLA_DQB1		HLA_DPB1		HLA_DRB1		HLA_DPA1		HLA_DQA1		Number of matching HLA homo	HLA-retyping	Age	Gender
THTC-01	A*33:03	-	B*58:01	-	C*03:02	-	DQB1*02:01	-	DPB1*04:01	-	DRB1*03:01	-	DPA1*01:03	-	DQA1*05:01	-	8	Matched	53	F
THTC-02	A*02:07	-	B*46:01	-	C*01:02	-	DQB1*06:01	-	DPB1*19:01	-	DRB1*08:03	-	DPA1*02:07	-	DQA1*01:03	-	8	Matched	49	F
THTC-03	A*11:01	-	B*13:01	-	C*03:04	-	DQB1*05:02	-	DPB1*13:01/107:01	-	DRB1*16:02	-	DPA1*02:02	-	DQA1*01:02	-	8	Matched	54	M
THTC-04	A*02:01	-	B*40:01	-	C*15:02	-	DQB1*03:01	-	DPB1*05:01	-	DRB1*11:01	-	DPA1*02:02	-	DQA1*05:05	-	8	Matched	76	F
THTC-05	A*33:03	-	B*58:01	-	C*03:02	-	DQB1*02:01	-	DPB1*04:01	-	DRB1*03:01	-	DPA1*01:03	-	DQA1*05:01	-	8	Matched	47	F
THTC-06	A*02:01	-	B*40:01	-	C*15:02	-	DQB1*03:01	-	DPB1*05:01	-	DRB1*11:01	-	DPA1*02:02	-	DQA1*05:05	-	8	Matched	40	M
THTC-11	A*02:01	A*33:03	B*58:01		C*03:02	-	DQB1*02:01	-	DPB1*04:01	-	DRB1*03:01	-	DPA1*01:03	-	DQA1*05:01	-	7	Matched	43	M
THTC-07	A*11:01	-	B*39:01	-	C*07:02	-	DQB1*06:01	-	DPB1*03:01	DPB1*05:01	DRB1*08:03	-	DPA1*01:03	DPA1*02:02	DQA1*01:03	-	6	Matched	40	F
THTC-08	A*33:03	-	B*58:01	-	C*03:02	-	DQB1*02:01	-	DPB1*04:01	DPB1*05:01	DRB1*03:01	-	DPA1*01:03	DPA1*02:02	DQA1*05:01	-	6	Matched	31	F
THTC-09	A*33:03	-	B*58:01	-	C*03:02	-	DQB1*02:01	-	DPB1*02:01	DPB1*05:01	DRB1*03:01	-	DPA1*01:03	DPA1*02:02	DQA1*05:01	-	6	Matched	37	F
THTC-10	A*02:07	A*11:01	B*46:01	-	C*01:02	-	DQB1*03:03	-	DPB1*05:01	-	DRB1*09:01	-	DPA1*04:01	DPA1*02:02	DQA1*03:02	-	6	Matched	53	M
THTC-12	A*33:03	-	B*58:01		C*03:02	-	DQB1*02:01	-	DPB1*04:01	'B1*13:01/107:	DRB1*03:01		DPA1*01:03	DPA1*02:01	DQA1*05:01	-	6	Matched	46	F
THTC-13	A*02:07	-	B*46:01	-	C*01:02	-	DQB1*03:03	-	DPB1*02:01	DPB1*05:01	DRB1*09:01	-	DPA1*01:03	DPA1*02:02	DQA1*03:02	-	6	Matched	34	M

Table S2. Ranking of HLA-homozygous iPSC haplotype in Taiwan, related to Figure 2.

Rank of haplotype freq.	Cell line	HLA haplotype HLA_A, HLA-B, HLA-DRB1
1	THTC-01	A*33:03-B*58:01-DRB1*03:01
1	THTC-05	A*33:03-B*58:01-DRB1*03:01
1	THTC-08	A*33:03-B*58:01-DRB1*03:01
1	THTC-09	A*33:03-B*58:01-DRB1*03:01
1	THTC-12	A*33:03-B*58:01-DRB1*03:01
2	THTC-10	A*02:07/A*11:01-B*46:01-DRB1*09:01
2	THTC-13	A*02:07-B*46:01-DRB1*09:01
3	THTC-02	A*02:07-B*46:01-DRB1*08:03
4	THTC-04	A*02:01-B*40:01-DRB1*11:01
4	THTC-06	A*02:01-B*40:01-DRB1*11:01
5	THTC-03	A*11:01-B*13:01-DRB1*16:02
NA#	THTC-07	A*11:01-B*39:01-DRB1*08:03
NA#	THTC-11	A*02:01/A*33:03-B*58:01-DRB1*03:01

#: no data available

Table S3. Potential cardiotoxic compounds identified from the primary high-content drug screen, related to Figure 3.

Compound	Cell lines													Number of cell lines with the identified hit
	THTC-01	THTC-02	THTC-03	THTC-04	THTC-05	THTC-06	THTC-07	THTC-08	THTC-09	THTC-10	THTC-11	THTC-12	THTC-13	
Dithiazanine iodide	V	V	V	V	V	V	V	V	V	V	V	V	V	13
Pyrvinium Pamoate	V	V	V	V	V	V	V	V		V	V	V	V	12
Didrovaltrate	V	V	V	V	V	V	V	V			V			9
Topotecan:Prestw-1196	V	V	V		V		V	V	V	V			V	9
Valtrate	V	V		V		V	V	V	V		V		V	9
Doxorubicin	V			V	V	V		V	V	V	V		V	9
Pararosaniline pamoate	V		V	V	V	V	V	V			V			8
Doxycycline	V	V	V		V		V	V	V	V				8
Daunorubicin	V		V	V	V	V				V	V			7
Demeclocycline	V	V			V		V	V	V				V	7
Meclocycline sulfosalicylate	V	V			V			V	V	V			V	7
Idarubicin	V		V	V	V	V					V	V		7
Lapatinib		V	V				V	V	V				V	6
Corynanthine (Yohimbine)				V	V	V					V			4
Cetrorelix		V					V		V	V				4
Ethacridine lactate		V					V			V				3

Table S4. Validated cardiotoxic compounds classified by their clinical indication, related to Figure 3.

Indication	Drug Name	Disease
Antibiotic	Pyrvinium	Antihelmintic drug
	Ethacridine Lactate	Antiseptic
Cancer	Didrovaltrate	Kidney, oral cavity, breast, and lung cancer
	Doxorubicin	Chemotherapy drug
	Daunorubicin	Chemotherapy drug
	Lapatinib	Breast cancer, solid tumors
	Idarubicin	Chemotherapy drug
Hormone Therapy	Cetrorelix	Gonadotropin-releasing hormone antagonist activity
Psychiatric	Valtrate	Mood disorders

Table S5. Potential neurotoxic compounds identified from the primary high-throughput drug screen, related to Figure 5.

Compound	Cell lines													Number of cell lines with the identified hit
	THTC-01	THTC-02	THTC-03	THTC-04	THTC-05	THTC-06	THTC-07	THTC-08	THTC-09	THTC-10	THTC-11	THTC-12	THTC-13	
Terfenadine	V	V	V	V	V	V	V	V	V	V	V	V	V	13
Dronedarone	V	V	V	V	V	V	V	V	V	V	V	V	V	13
Hexetidine	V	V	V	V	V	V	V	V	V	V	V	V	V	13
Penfluridol	V		V	V	V	V	V	V	V	V	V	V	V	12
Moxidectin	V	V	V	V		V	V	V	V	V	V	V	V	12
Tegaserod	V	V		V	V		V	V	V	V	V	V	V	11
Ceritinib	V	V		V		V	V	V	V	V	V		V	10
Clofoctol	V		V	V		V	V	V	V	V	V		V	10
Selamectin	V			V		V	V	V	V	V	V		V	9
Zinc pyrithione	V		V	V	V	V	V		V		V		V	9
Mitoxantrone	V	V		V	V	V	V		V		V	V		9
Telotristat ethyl		V	V	V	V	V		V			V			7
Octenidine Dihydrochloride	V	V		V			V		V		V		V	7
Pacritinib	V	V	V			V	V			V				6
Lomitapide	V		V	V			V				V		V	6
Entrectinib	V		V	V		V					V		V	6
Tetrandrine		V			V			V		V		V		5
Crizotinib		V			V			V		V		V		5
Berbamine		V			V			V		V		V		5
Sunitinib			V		V			V		V	V			5
Fedratinib	V		V	V	V			V						5
Visomitin	V	V				V			V		V			5
Gramicidin	V			V			V		V		V			5
Netupitant									V	V	V		V	4
Salmeterol		V			V								V	3
Domiphen	V			V	V				V					4
Fingolimod		V							V		V		V	4
Tubercidin			V			V	V		V					4
Ebastine			V			V							V	3
Amiodarone			V	V		V								3

Table S6. Validated neurotoxic compounds classified by their clinical indication, related to Figure 5.

Indication	Drug Name	Disease
Antibiotic	Clofoctol	Gram-Positive Bacteria Infected
	Domiphen Bromide	Pharyngitis, thrush and mouth ulcers
	Gramicidin A	Transplant rejection
	Octenidine Dihydrochloride	Antibiosis
	Zinc Pyrithione	Seborrhoeic Dermatitis
	Tubercidin	Antibiotics
Cancer	Crizotinib	Non-small cell lung cancer
	Ceritinib	Non-small cell lung cancer
	Entrectinib	Solid tumours
	Fedratinib	Primary or secondary myelofibrosis
	Pacritinib	Post-essential thrombocythaemia myelofibrosis
	Sunitinib	Gastrointestinal stromal tumours; Pancreatic cancer; Renal cell carcinoma
	Telotristat Ethyl	Malignant carcinoid syndrome
	Visomitin	Pancreatic cancer
Cardiovascular	Amiodarone	Ventricular Fibrillation; Ventricular Tachycardia
	Dronedarone	Atrial Fibrillation; Atrial Flutter
Infection	Moxidectin	Onchocerciasis
	Selamectin	Ectozoic parasite
Nervous system	Fingolimod	Multiple sclerosis
	Penfluridol	Schizophrenia
Digestive system	Tegaserod	Constipation; Irritable bowel syndrome
Immune system	Ebastine	Allergic Conjunctivitis; Allergic Rhinitis; Urticaria
Metabolism	Lomitapide	Hyperlipoproteinaemia type IIa

Table S7. Primers used in PCR experiments, related to STAR Methods.

Target		Sequence
SeV	Forward	GGATCACTAGGTGATATCGAGC
	Reverse	ACCAGACAAGAGTTTAAGAGATATGTATC
KOS	Forward	ATGCACCGCTACGACGTGAGCGC
	Reverse	ACCTTGACAATCCTGATGTGG
Klf4	Forward	TTCCTGCATGCCAGAGGAGCCC
	Reverse	AATGTATCGAAGGTGCTCAA
c-Myc	Forward	TAACTGACTAGCAGGCTTGTCG
	Reverse	TCCACATACAGTCCTGGATGATGATG
Actin	Forward	CCCTGGACTTCGAGCAAGAG
	Reverse	ACTCCATGCCCAGGAAGGAA